

Causes of growing middle-upper tropospheric ozone over the Northwest Pacific region

Xiaodan Ma^{1,2}, Jianping Huang^{3,4}, Michaela I. Hegglin^{2,5}, Patrick Jöckel⁶, and Tianliang Zhao¹

¹Collaborative Innovation Center on Forecast and Evaluation of Meteorological Disasters, Key Laboratory for Aerosol-Cloud-Precipitation of China Meteorological Administration, Nanjing University of Information Science and Technology, Nanjing 210044, China.

²Institute of Energy and Climate Research – Stratosphere (IEK-7), Forschungszentrum Jülich, Jülich, Germany.

³Environmental Modeling Center, NOAA National Centers for Environmental Prediction, College Park, MD, USA.

⁴Center for Spatial Information Science and Systems, College of Science, George Mason University, Fairfax, VA 22030, USA.

⁵Department of Meteorology, University of Reading, Reading, United Kingdom

⁶Deutsches Zentrum für Luft- und Raumfahrt (DLR), Institut für Physik der Atmosphäre, Oberpfaffenhofen, Germany

Correspondence to: Jianping Huang (jianping.huang@noaa.gov)

Abstract. Long-term ozone (O₃) changes in the middle to upper troposphere are critical to climate radiative forcing and tropospheric O₃ pollution. Yet, these changes remain poorly quantified through observations in East Asia. Concerns also persist regarding the data quality of the ozonesondes available at the World Ozone and Ultraviolet Data Center (WOUDC) for this region. This study aims to address these gaps by analyzing O₃ soundings at four sites along the northwestern Pacific coastal region over the past three decades, and assessing their consistency with an atmospheric chemistry-climate model simulation. Utilizing the European Centre for Medium-Range Weather Forecasts (ECMWF) – Hamburg (ECHAM)/Modular Earth Submodel System (MESSy) Atmospheric Chemistry (EMAC) nudged simulations, it is demonstrated that trends between model and ozonesonde measurements are overall consistent, thereby gaining confidence in the model’s ability to simulate O₃ trends and confirming the utility of potentially imperfect observational data. A notable increase in O₃ mixing ratio around 0.29-0.82 ppb a⁻¹ extending from the middle to upper troposphere is observed in both observations and model simulations between 1990 and 2020, primarily during spring and summer. The timing of these O₃ tongues is delayed when moving from south to north along the measurement sites, transitioning from late spring to summer. Investigation into the drivers of these trends using tagged model tracers reveals that O₃ of stratospheric origin (O₃S) dominates the absolute O₃ mixing ratios over the middle-to-upper troposphere in the subtropics, contributing to the observed O₃ increases by up to 96% (40%) during winter (summer), whereas O₃ of tropospheric origin (O₃T) governs the absolute value throughout the tropical troposphere and contributes generally much more than 60% to the positive O₃ changes, especially during summer and autumn. During winter and spring, a decrease of O₃S is partly counterbalanced by an increase of O₃T in the tropical troposphere. This study highlights that the enhanced downward transport of stratospheric O₃ into the troposphere in the subtropics and a surge of tropospheric source O₃ in the tropics are the two key factors driving the enhancement of O₃ in the middle-upper troposphere along the Northwest Pacific region.

Keywords: EMAC model, ozone sounding, stratospheric intrusion, tropospheric ozone

41 **1. Introduction**

42 Stratospheric intrusions and photochemical production are two major contributors to tropospheric ozone (O₃, Ding
43 and Wang, 2006; Neu et al., 2014; Williams et al., 2019; Zhao et al., 2021). The stratosphere accommodates 90%
44 of the total O₃ in the atmosphere. As the largest natural source, downward transport of O₃-enriched air from the
45 stratosphere exerts an important impact particularly on the seasonality of tropospheric O₃ (Williams et al., 2019).
46 Free tropospheric O₃ increases of 7% (measured as a partial column between 3-9 km) between 2005 and 2010 over
47 China have been identified as a consequence of increased O₃ precursor emissions and enhanced downward
48 transport from stratospheric O₃ (Verstraeten et al., 2015). While photochemical production is highly dependent on
49 anthropogenic emissions, the impact of stratospheric intrusions on tropospheric O₃ is mainly governed by inter-
50 annual variability and climate-driven changes in the atmospheric circulation (Neu et al., 2014; Albers et al., 2018).
51 Compared to the spatio-temporal variations of O₃ in the lower troposphere, the evolution in the middle-upper
52 troposphere and their underlying causes remain inadequately quantified, largely due to scarcity of long-term,
53 vertically resolved observational data.

54
55 Chemistry-climate modeling studies demonstrate that climate variability in the atmospheric circulation such as an
56 enhanced Brewer-Dobson circulation (BDC) can promote greater seasonal build-up of O₃ in the extratropical
57 lowermost stratosphere during winter (Ray et al., 1999; Sudo et al., 2003; Konopka et al., 2015; Ploeger & Birner,
58 2016; Young et al., 2018; Akritidis et al., 2019; Griffiths et al., 2020; Liao et al., 2021). Subsequent stratospheric
59 intrusions can then lead to the increased stratosphere-troposphere exchange of O₃ as a result of this enrichment,
60 particularly in spring when the lowermost stratospheric reservoir of O₃ reservoir reaches its annual maximum and
61 is seasonally “flushed” thereafter (Hegglin and Shepherd, 2007; Bönisch et al., 2009). However, this process
62 depends on changes in the BDC's deep and shallow branches. Strengthening of the deep branch increases
63 lowermost stratospheric O₃ while strengthening of the shallow branch favors enhanced transport and mixing of
64 low-O₃ air from the tropical upper troposphere (Plumb, 2002; Bönisch et al., 2009). A study using a coupled
65 atmosphere-ocean model with interactive stratospheric chemistry projects a 20–30% increase in global
66 stratosphere-to-troposphere transport (STT) O₃ flux from 1965 to 2095, as the result of an accelerated stratospheric
67 BDC under an intermediate climate change scenario (Hegglin and Shepherd, 2009). Furthermore, chemistry-
68 climate models (CCMs) predict an even larger increase of the STT O₃ flux (25–80%) under climate change
69 scenarios such as RCP8.5 (Collins, 2003; Sudo et al., 2003; Meul et al., 2018). Notably, Williams et al. (2019)
70 identified an enhanced STT O₃ over Asia and the Pacific region during 1980-2010 based on two different CCMs.
71 The shallow branch of BDC is associated with the breaking of synoptic and planetary-scale waves in the
72 subtropical lower stratosphere (Plumb, 2002; Birner and Bönisch, 2011). Several small-scale processes in
73 proximity to the tropopause lead to irreversible STT events, including Rossby wave breaking, tropospheric
74 cyclones, cut-off lows, and tropopause folding events (Holton et al., 1995). On a regional basis, including East
75 Asia and its coastal area, subtropical westerly jets modulate the location, timing, and frequency of tropopause folds
76 (Sprenger et al., 2003; Albers et al., 2018). Satellite measurements of O₃ and water vapor over six years were used
77 to quantify the impact of a changing stratospheric circulation on tropospheric O₃ in the northern hemisphere (Neu
78 et al., 2014). These observation-based results support the modeling studies that the intensified stratospheric BDC
79 tends to enhance the impact of the stratospheric intrusions on tropospheric O₃. However, the conclusions drawn

80 from the numerical studies have not yet been validated through long-term O₃ measurements, particularly O₃-
81 sounding data (Trickl et al., 2011).

82

83 From 1990 onwards, a significant amount of the anthropogenic emissions responsible for O₃ formation have shifted
84 from North America and Europe to Asia (Granier et al., 2011; Cooper et al., 2014; Zhang et al., 2016). In East
85 Asia, the overall long-term trend of the daytime average near-surface O₃ is 0.45 ppb a⁻¹, contrasting with a trend
86 of -0.28 ppb a⁻¹ in North America in the summertime (April-September) during 2000-2014 (Chang et al., 2017).
87 Several studies have documented the increase in emissions of O₃ precursors at few sites available for evaluating
88 the long-term trends across East Asia (Ma et al., 2016; Sun et al., 2016; Xu et al., 2016; Wang et al., 2017). On
89 the other hand, some regions in East Asia have seen a decline in precursor emissions after 2004, such as Beijing,
90 Hong Kong, and Japan due to local emission control efforts (Krotkov et al., 2016; Liu et al., 2016; Miyazaki et al.,
91 2017; van der A et al., 2017). Elevated NO₂ emissions over megacities in China were possibly transported to Japan,
92 potentially offsetting the local emission control efforts (Duncan et al., 2016). Further research is required to
93 understand the long-term changes in tropospheric O₃, especially in East Asia, where rapid economic growth
94 coincides with strict environmental regulations.

95

96 In this study, we present thirty years of O₃ observations from balloon soundings with a focus on latitudinal
97 differences. To this end, observations from four sounding sites are analyzed together with model simulation results
98 to quantify the long-term trends of middle-upper tropospheric O₃ and contributions of different origins along the
99 northwestern Pacific coastal region. We are particularly interested in the regional difference near 30°N, the
100 transition zone between the Hadley and Ferrel circulation cells, where the subtropical jet (STJ) prevails and
101 tropopause folding is frequently observed (Škerlak et al., 2015; Zhao et al., 2021). The specific questions to be
102 addressed by this study are 1) How do O₃ trends in the middle-upper troposphere vary with latitude and season
103 over the northwestern Pacific coastal regions and are these observed trends consistent with those derived from a
104 chemistry-climate model? 2) To what extent are these tropospheric O₃ changes linked to stratospheric influences?
105 And 3) to what extent are these tropospheric O₃ changes linked to tropospheric sources, i.e. photochemical O₃
106 production due to biogenic and anthropogenic precursor emissions? The study aims to provide observational
107 evidence to validate and constrain the CCMs' predictions of climate-change impact on tropospheric O₃ in East
108 Asia (e.g., Williams et al., 2019) where such information is still lacking.

109

110 **2. Data and method**

111 **2.1 Ozonesonde observations**

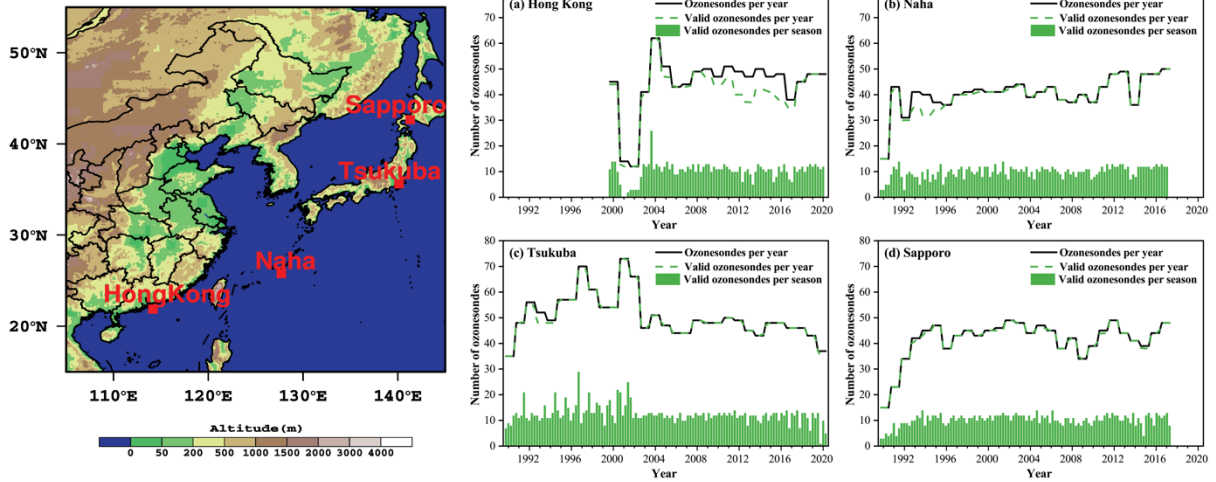
112 Around thirty years of O₃-sounding data at four sites along the northwestern Pacific coastal regions (Sapporo,
113 Tsukuba, Naha, and Hong Kong) are used to characterize spatiotemporal variations of O₃ in the troposphere.
114 Ozonesondes were launched around 14:00 local standard time (LST) once a week, which corresponds to the time
115 when photochemical production reaches its daily maximum (Oltmans et al., 2004). The ozonesonde measurements
116 include O₃ partial pressure, temperature, relative humidity, wind speed, and wind direction. Vertical O₃
117 measurements range from the surface to the middle stratosphere approaching 30 km. The Hong Kong site has
118 continually operated the electrochemical concentration cell (ECC) instrument since the beginning of its record.
119 For the three sites in Japan, the O₃-sounding data were measured by Carbon-iodine (CI) ozonesondes with 10-

120 second recording intervals before 2009 and changed to the ECC instrument with 2-second recording intervals. The
121 operating principle of CI ozonesondes and ECC ozonesondes both are based on the reaction of O₃ to potassium
122 iodide solution wherein free iodine is liberated (Johnson et al., 2002; Witte et al., 2018). However, the transition
123 of the measurement technology from CI to ECC around 2009 led to uncertainties and an overestimation of the
124 long-term O₃ trends due to a step-change in the resulting timeseries (Figure S1). Cross-evaluation of OMI data
125 and the ozonesonde observation at the Japan sites indeed showed that CI ozonesonde measurements of
126 tropospheric O₃ columns are negatively biased relative to ECC measurements by 2–4 DU compared with the OMI
127 data (Bak et al., 2019). A correction factor was applied to the O₃ profiles during the CI measurement period to
128 remedy the problem. However, the applied factors were found to inaccurately impact observed tropospheric O₃
129 values (Morris et al., 2013). Removing the correction factor in the CI measurements can improve the consistency
130 of ozonesondes with OMI data (Morris et al. 2013). We thus removed the correction factor applied to the original
131 ozonesonde data available from the WOUDC for these three Japanese-sounding stations hereinafter. After
132 removing the correction factors during the observation period, the corrected datasets show no notable step-changes
133 around 2009 at the Japanese sites anymore (Figure S2). It is worth noting that the conclusion we draw from current
134 available long-term ozonesonde observations has limitations on the long-term trends but still has important
135 implications on the understanding of tropospheric O₃ changes and model evaluations. The weekly launch
136 frequency of the ozonesondes has been validated as reliable in representing long-term O₃ trends, as evidenced by
137 comparing them with near-surface O₃ trends at hourly time resolution (Liao et al., 2021). A summary of
138 ozonesonde-site location and data availability is presented in Table 1 and Figure 1.

139
140 We limit our analyses of tropospheric and lower-stratospheric O₃ profiles to altitudes below 18 km and remove
141 duplicate O₃ values during the descent period at the same heights in the time series to prevent redundant
142 measurements as well as to reduce the uncertainty of solution evaporation and loss due to the O₃ sounding balloon
143 bursting and/or tumbling through the atmosphere. O₃ profiles with continuous data missing more than a 200m
144 vertical coverage are excluded. The selected valid O₃ profiles with 10s or 2s recording intervals are linearly
145 interpolated into 10m vertical intervals and then averaged into 50m data points. The O₃ profiles after the quality
146 control with 50m vertical resolution are used for further analysis.

147
148 Due to the latitudinal differences and the seasonal variations in tropopause height across the four O₃-sounding
149 observation sites, it is inappropriate to apply a specific height as the tropopause height. We thus employ the World
150 Meteorological Organization lapse rate tropopause definition to calculate the tropopause height (hereafter called
151 Z_t) for each site and O₃ profile. The Z_t is defined as the level at which the lapse rate decreases to 2 K km⁻¹ or less,
152 provided that the average lapse rate between this level and all higher levels within 2 km does not exceed 2 K km⁻¹
153 (WMO, 1957).

154
155 To better compare O₃ levels and trends at different latitudes within the troposphere, we normalize the height of
156 each O₃ profile into 0~1 by dividing the altitude by the tropopause height Z_t. The upper troposphere (UT) is then
157 defined by the normalized height (Z/Z_t) range between 0.7 and 0.9. The middle troposphere (MT) and lower
158 troposphere (LT) are 0.4~0.6 and 0~0.2 Z/Z_t, respectively.



159

160 Figure 1. Location of O₃-sounding sites and seasonal and annual ozonesonde sampling at a) Hong Kong, (b) Naha, (c)
 161 Tsukuba, and (d) Sapporo. The continuous line shows the number of ozonesondes launched per year. The bars show
 162 the corresponding number per season. The dashed line indicates the number of valid ozonesondes reaching up to 18 km
 163 altitude.

164 Table 1. Location of O₃-sounding sites, measurement periods, and total data available along the northwestern Pacific
 165 coastal region.

Station	Latitude	Longitude	Elevation (m)	Period	Total data	Valid data (18km)
Sapporo	43.10°N	141.30°E	19	1990-2017	1167	1159(99%)
Tsukuba	36.06°N	140.13°E	31	1990-2020	1564	1556(99%)
Naha	26.20°N	127.70°E	27	1990-2017	1137	1114(98%)
Hong Kong	22.31°N	114.17°E	66	2000-2020	929	863(93%)

166

167 2.2 EMAC model and simulation setup

168 In this study, the European Centre for Medium-Range Weather Forecasts (ECMWF) – Hamburg
 169 (ECHAM)/Modular Earth Submodel System (MESSy) Atmospheric Chemistry (EMAC) model is utilized to
 170 investigate the long-term changes of tropospheric O₃ and to quantify the relative contributions of different driving
 171 factors. The EMAC model is a global model that considers the interaction of chemistry and dynamic processes
 172 between the surface and the middle atmosphere (Jöckel et al., 2016). The reference simulation with specific
 173 dynamics (REF-D1) results from the EMAC model are used in this study (Jöckel et al., 2024a; Jöckel et al., 2024b).
 174 The REF-D1 experiment is a hindcast simulation of the atmospheric state, using a prescribed sea surface
 175 temperature and sea ice from observations along with forcing for the extra-terrestrial solar flux, long-lived
 176 greenhouse gasses, and O₃-depleting substances, stratospheric aerosols, and an imposed quasi-biennial oscillation
 177 that approximate the observed variations over the historical period to the fullest extent possible. The hindcast
 178 simulations are performed from 1980 to 2019 with the specific dynamics nudging by Newtonian relaxation towards
 179 ECMWF ERA-5 reanalysis meteorological data (Hersbach et al., 2020), including temperature, logarithm of
 180 surface pressure, divergence, and vorticity.

181

182 The simulations are conducted at a T42 (triangular) spectral resolution corresponding to an approximately 2.8° ×
 183 2.8° quadratic Gaussian grid, 90 hybrid sigma pressure vertical levels from surface up to 0.01 hPa, and with a 720s
 184 time step length (Jöckel et al., 2016). EMAC uses chemical submodels, the Module Efficiently Calculating the

185 Chemistry of Atmosphere (MECCA, Sander et al., 2011) and the scavenging submodel (SCAV, Tost et al., 2006)
186 to describe comprehensive chemical reaction mechanisms in gas and liquid phases that include O₃, CH₄, HO_x and
187 NO_x chemistry, non-methane hydrocarbon (NMHC) chemistry up to C₄ and isoprene, halogen (Cl and Br)
188 chemistry, and sulfur chemistry.

189
190 Emissions of lightning NO_x, soil NO_x, and isoprene (C₅H₈) are calculated online for EMAC using the submodels
191 LNO_x (Tost et al., 2007) and online-emissions (ONEMIS) (Kerkweg et al., 2006; Jöckel et al., 2016), respectively.
192 EMAC simulates the photolysis (submodel JVAL, Sander et al., 2014) and shortwave radiation schemes
193 (FUBRAD, Kunze et al., 2014) consistently, with particular regard to the evolution of the 11-year solar cycle
194 (Morgenstern et al., 2017). For anthropogenic emissions, mixing ratios of greenhouse gases, O₃-depleting
195 substances (ODS), and other boundary conditions, the EMAC model setup follows the Chemistry–Climate Model
196 Initiative (CCMI) 2020 protocol of the refD1 hindcast simulations (SPARC, 2021).

197
198 The EMAC model provides the diagnostic tracer O₃S to directly measure the stratosphere-to-troposphere exchange
199 of O₃. The O₃S tracer is transported across the tropopause into the troposphere and is removed by tropospheric O₃
200 reactions (Jöckel et al., 2006; Jöckel et al., 2016). When O₃S re-enters the stratosphere, it is re-initialized (Roelofs
201 and Lelieveld, 1997). The tropospheric O₃ source (O₃T) is here calculated as tropospheric O₃ minus stratospheric
202 O₃ ($O_3T = O_3 - O_3S$).

203
204 To better compare the model results with the observations, the simulation data is extracted from the grid boxes
205 nearest to the observation sites. Specifically, 200 hPa is chosen for Hong Kong and Naha, and 400 hPa for Tsukuba
206 and Sapporo to represent the upper troposphere. The middle troposphere is defined at 500hPa, while the lower
207 troposphere is represented by 850 hPa in the model results. To assess the statistical significance of the differences,
208 a paired two-sided t-test ($p < 0.05$) is conducted for comparison.

209

210 **3. Results**

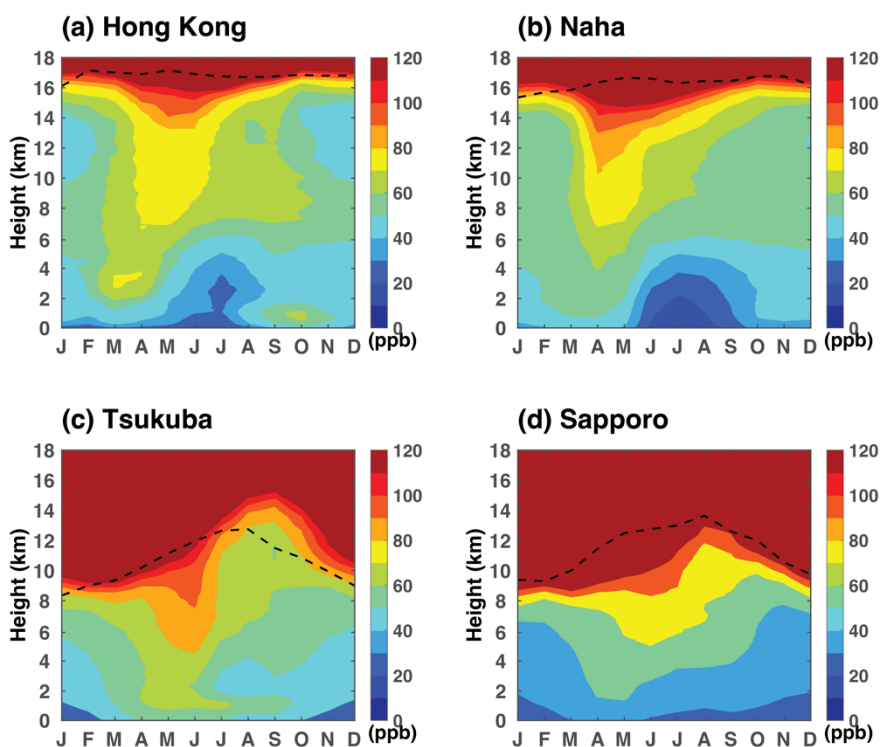
211 **3.1 Observational changes at different stations**

212 **3.1.1 Climatological distribution of tropospheric O₃**

213 Figure 2 depicts the monthly climatological vertically resolved tropospheric O₃ distribution throughout the year.
214 The four sites all show a distinct tongue-shaped pattern in top-down direction characterized by high concentrations
215 of O₃ greater than 70 ppb, each exhibiting peak levels in distinct months. The O₃ tongue extends from the lower
216 stratosphere to the middle troposphere, even further spreading downward to the lower troposphere. In subtropical
217 regions such as Hong Kong and Naha, the O₃ tongue starts to appear in early spring. Their appearance becomes
218 progressively delayed when moving towards higher latitudes, with peak occurrences observed in Tsukuba during
219 June and Sapporo in July (Figure 2c-d). For the mid-latitudes over the Pacific region, the incidence of stratospheric
220 intrusions has been found to have a strong correlation with the location of the STJ (Zhao et al., 2021). The
221 northward shift of the STJ with seasons agrees well with the occurrence of the O₃ tongues in different months over
222 the four sites along the northwest Pacific coastal regions (Figure S3). Tropopause folding events are located
223 preferentially on the southern flank of the STJ, with the associated stratosphere-to-troposphere transport of O₃ thus
224 potentially contributing to the observed seasonal lag in the occurrence of the O₃ tongues (Figure S4).

225

226 On the other hand, the four sites display distinct month-height cross-section distribution patterns of O₃. In near-
 227 tropical regions such as Hong Kong and Naha during the summer, a relatively "clean" layer with O₃ mixing ratios
 228 less than 40 ppbv extends from the surface to about 5.0 km above the ground level (AGL). Such a structure,
 229 characterized by low concentrations in the lower troposphere is not observed at the other two high-latitude sites.
 230 The unfavorable meteorological conditions linked to the East Asian monsoon such as a strong wind, precipitation,
 231 and less radiation could lead to significant O₃ scavenging and less photochemical production. This suggests that
 232 the East Asian summer monsoon has a more significant impact on O₃ vertical structures at lower latitude sites
 233 compared to high latitude sites. Meanwhile, it is noticed that high O₃ mixing ratios appear within the atmospheric
 234 boundary layer (ABL) (0.7-1.6km according to Su et al., (2017)) in Hong Kong in autumn (Figure 2a), which
 235 represents the combined effect of local emissions and regional transport. During this season, the prevailing winds
 236 are predominantly from northwest to north, which could bring elevated levels of O₃ and its precursors from the
 237 Pearl River Delta region, a major manufacturing base in China, to Hong Kong (Ding et al., 2013; Lin et al., 2021).



238
 239 **Figure 2. Month-height cross sections of monthly mean O₃ at four O₃-sounding sites, (a) Hong Kong, (b) Naha, (c)**
 240 **Tsukuba, and (d) Sapporo, from 1990 to 2017/2020 (2000 to 2020 for Hong Kong). Black dash lines indicate the multi-**
 241 **year average tropopause height calculated by observations according to the WMO lapse rate tropopause definition.**
 242

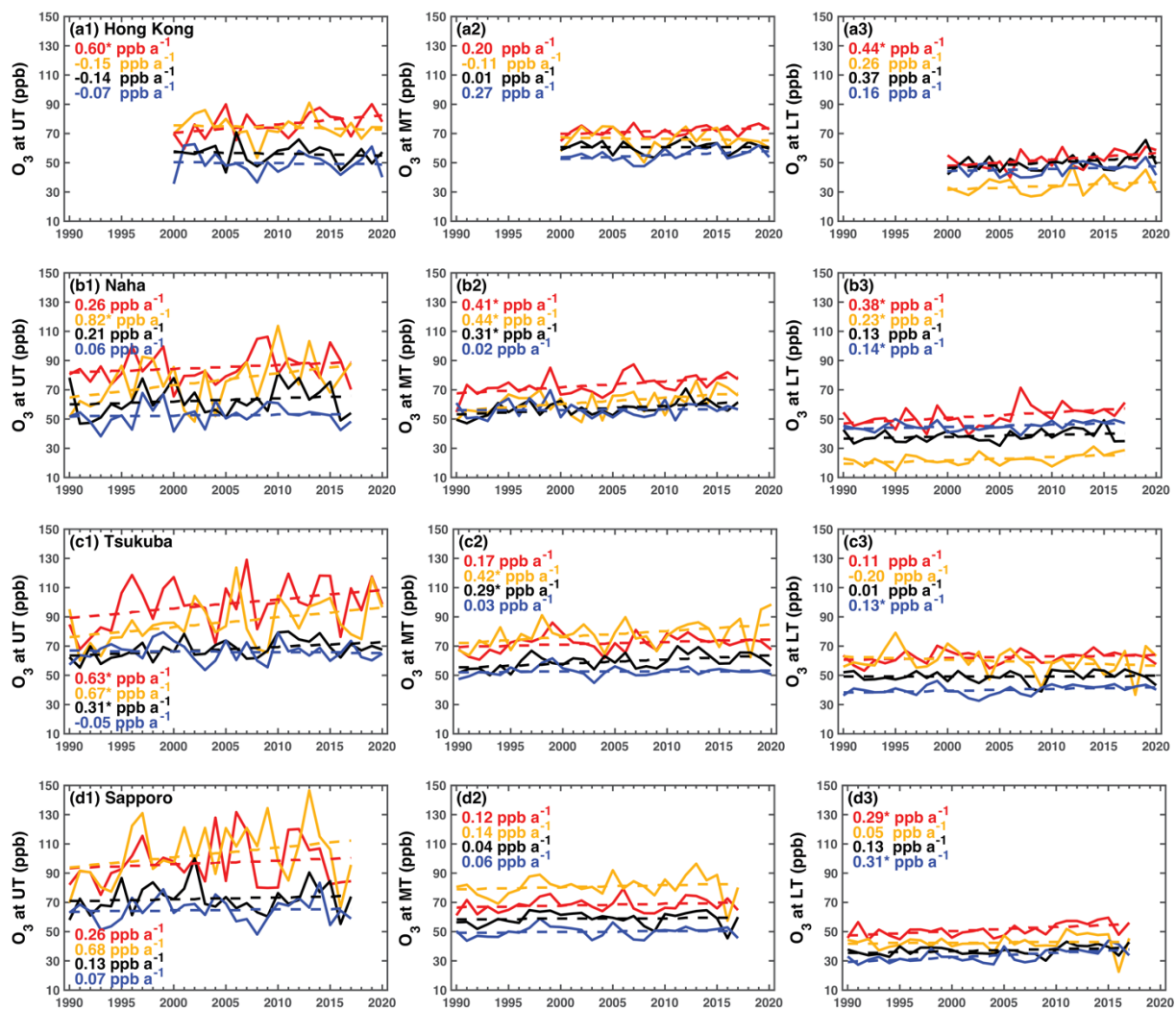
243 3.1.2 Long-term trends in different layers of the troposphere

244 Figure 3 presents the long-term trends of O₃ in the upper, middle, and lower troposphere. In general, O₃ in the
 245 upper troposphere shows larger increases during boreal spring and summer than autumn and winter among the
 246 four sites except for Hong Kong. The largest O₃ trends are observed at Naha with an increase of 0.82 ppb a⁻¹ during
 247 the summer and at Tsukuba (0.63 ppb a⁻¹) during the spring (at a 95% confidence level). Hong Kong only shows
 248 a significant O₃ increase in spring with 0.60 ppb a⁻¹ while Tsukuba exhibits extensive O₃ increase except winter.
 249 For the Sapporo site, substantial positive O₃ changes are observed during summer but not statistically significant
 250 due to large temporal variabilities. This finding implies the importance of STJ in the change of O₃ in the upper

251 troposphere at Naha and Tsukuba. The locations are situated within the transitional zone between the Hadley and
 252 Ferrel circulation cells in spring and summer, as illustrated in Figure S3. This influence appears more pronounced
 253 in comparison to the other two sites, namely Hong Kong and Sapporo, which are situated further from this
 254 transitional zone.

255
 256 Moving to the middle troposphere, Naha and Tsukuba consistently display an O₃ increase during all four seasons.
 257 The changes at these two sites in spring, summer, and autumn are more evident than those at the other two sites
 258 and winter. This suggests a potential strengthened contribution from regional transport and stratospheric intrusion
 259 for these two sites. In addition, lightning-produced NO_x emissions contribute to major events of O₃ in the middle-
 260 upper troposphere over convection active regions (Liu et al., 2002; Zhang et al, 2012). How those factors contribute
 261 to O₃ enhancement remains a question for further investigations.

262 In the lower troposphere, substantial O₃ increases are observed at all sites in spring except Tsukuba. O₃
 263 enhancement in the lower troposphere over Hong Kong during springtime is associated with either equatorial
 264 Northern Hemisphere biomass burning in Africa or Southeast Asian biomass burning (Oltmans et al., 2004). The
 265 Tsukuba site experienced a slight decrease in summer over the past three decades. Such a decrease could be
 266 primarily attributed to the changes in anthropogenic emissions in East Asia (Li et al, 2019).



267
 268 **Figure 3. Long-term changes of O₃ in the Upper Troposphere (defined as 0.7-0.9 tropopause normalized height, first**
 269 **column), Middle Troposphere (defined as 0.4-0.6 tropopause normalized height, second column), and Lower**

270 Troposphere (defined as 0-0.2 tropopause normalized height, third column) in boreal spring (MAM, red lines), summer
271 (JJA, yellow lines), autumn (SON, black lines), and winter (DJF, blue lines) at Hong Kong (a1-a3), Naha (b1-b3),
272 Tsukuba (c1-c3), and Sapporo (d1-d3). Trends with a star symbol (*) indicate significance at the 95% confidence level.
273

274 Overall, the long-term changes in tropospheric O₃ displayed considerable variability, contingent on the
275 atmospheric layers (i.e., low, middle, and upper) and the geographical latitude of observation sites. Naha, Tsukuba,
276 and Sapporo exhibited an increase in the middle-upper troposphere. A substantial rise is observed in the upper
277 troposphere during summer over Naha (0.82 ppb a⁻¹) and spring over Tsukuba (0.63 ppb a⁻¹). When compared to
278 the other three sites, changes in the middle-upper troposphere over Hong Kong are smaller or negative, except
279 during springtime. All four sites demonstrated an increase in O₃ mixing ratios across the four seasons in the lower
280 troposphere, except for summer in Tsukuba. Investigating the driving factors behind such differences in change
281 becomes one of the objectives of this study. A more comprehensive exploration of O₃ origin and their contributions
282 to the changes in tropospheric O₃ will be discussed in Section 3.2, leveraging modeling results to provide deeper
283 insight.

284

285 3.1.3 Changes in composite O₃ cross-sections between decades

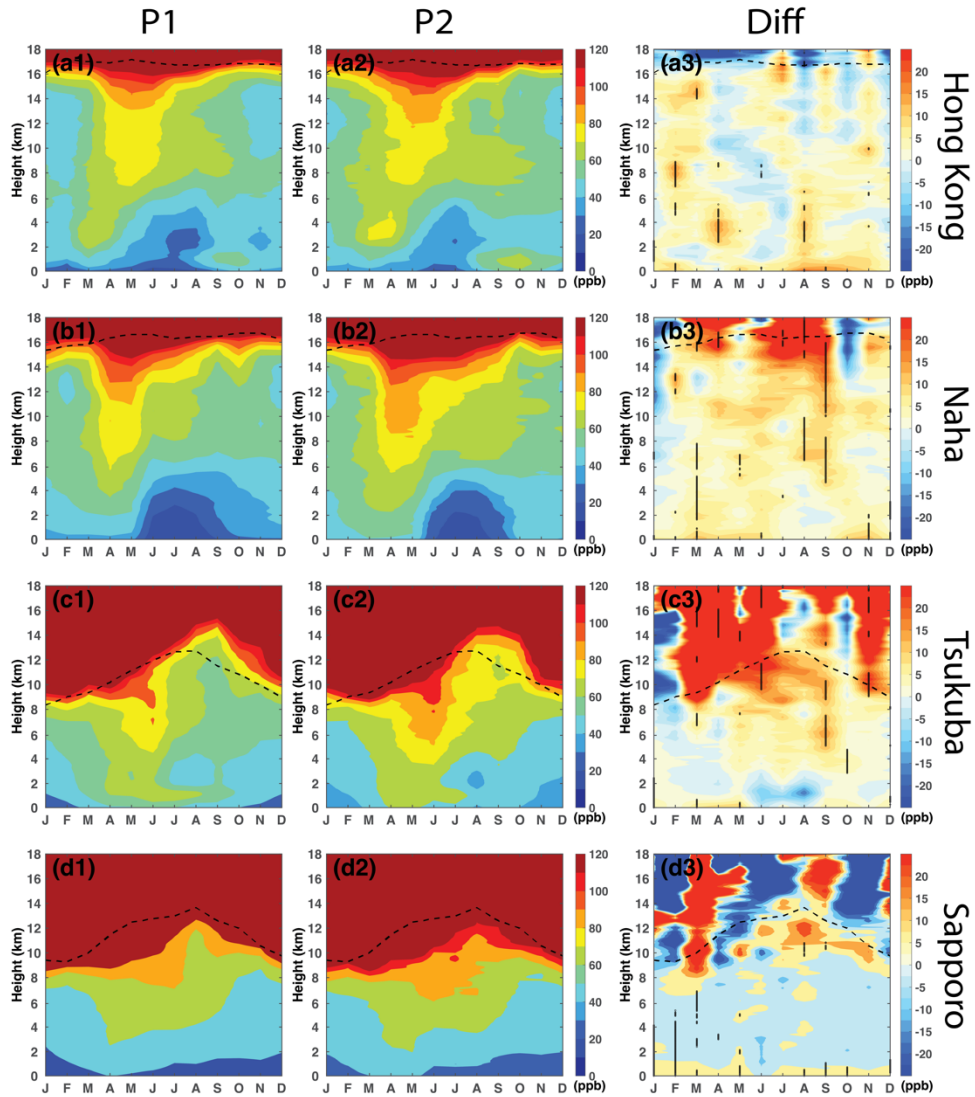
286 Tropospheric O₃ shows a larger variability in the upper troposphere compared to the middle and lower troposphere
287 (Figure 3 a1-d3). Such a large variability, likely driven by transport and dynamics in the tropopause region,
288 impedes drawing definite conclusions on long-term trends for single measurement sites with infrequent sampling.
289 Therefore, the aggregation of tropospheric O₃ during the early and late decades is expected to provide more robust
290 insights.

291

292 Figure 4 illustrates the vertically resolved tropospheric O₃ distributions and changes between the early (the 1990s
293 for Naha, Tsukuba, and Sapporo; the 2000s for Hong Kong) and late (2010s) decades as a function of the month.
294 Their respective tropospheric O₃ changes over the same period (i.e., 2000s to 2010s) at the four sites are presented
295 in Figure S5 to demonstrate the consistency of the results. The time lag pattern for the O₃ tongue remains the same
296 from April in the southern site of Hong Kong to July in the northern site of Sapporo for the first and the last
297 decades (Figure 4 a1-d1). However, there are noticeable increases in O₃ mixing ratios and a deeper layer extension
298 of the O₃ concentration greater than 80 ppbv from the stratosphere to the troposphere at Naha and Tsukuba over
299 the past several decades (Figure 4 a2-d2).

300

301 As illustrated in Figure 4 a3-d3, Naha, Tsukuba, and Sapporo exhibit significant enhancements of O₃ from the
302 middle-upper troposphere to the lowermost stratosphere. In contrast to the three sites in Japan, Hong Kong shows
303 more significant O₃ changes in the lower troposphere. The build-up of lowermost stratospheric (LMS) O₃ happens
304 from the winter to spring, thus the STE flux of O₃ normally reaches its peak during late spring to early summer in
305 the extratropical regions (e.g., Škerlak et al., 2015; Albers et al., 2018). The O₃ tongue during the spring and
306 summer is possibly associated with enhanced contribution from stratospheric intrusions. While it may be tempting
307 to conclude that such an O₃ increase primarily originates from the stratosphere due to their proximity, observational
308 data alone cannot provide a definite conclusion. Additionally, different locations among the four sites may
309 introduce further differences in O₃ sources.



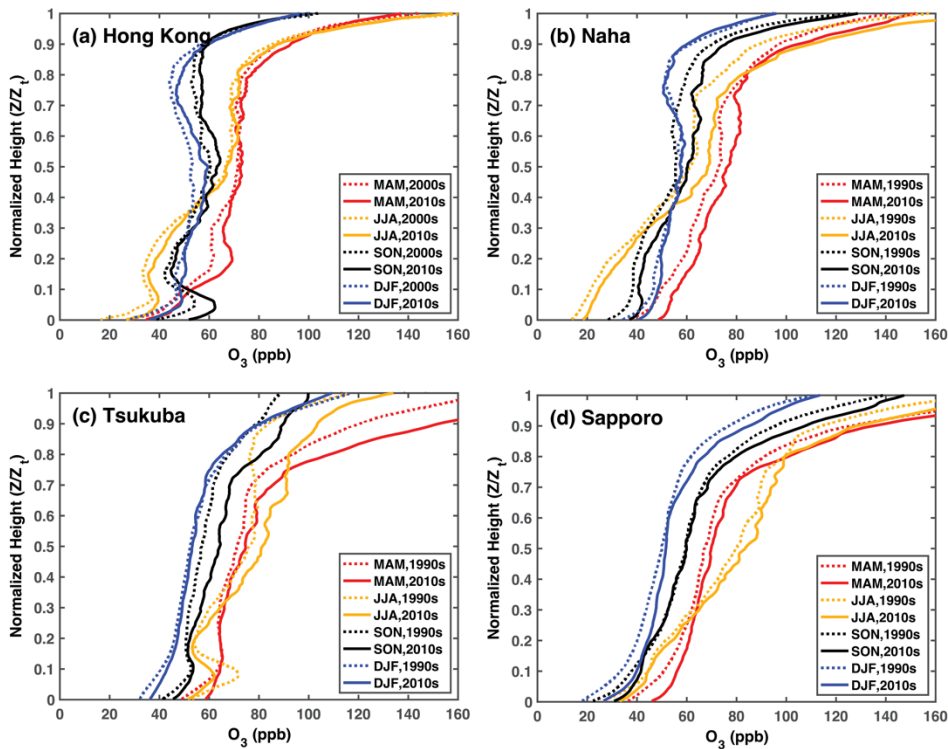
310
 311 **Figure 4. Month-height cross sections of monthly mean composite O₃ in the first period P1 (1990s for Naha, Tsukuba,**
 312 **and Sapporo, but 2000s for Hong Kong), the last period (P2: 2010s), and the differences of O₃ between P2 and P1 at**
 313 **(a1-a3) Hong Kong, (b1-b3) Naha, (c1-c3) Tsukuba and (d1-d3) Sapporo. Black dash lines indicate the tropopause**
 314 **heights calculated by observations according to the WMO lapse rate tropopause definition. Dashed lines in the a3-**
 315 **d3 represent the layer with statistically significant changes according to a paired two-sided t-test ($p < 0.05$).**
 316

317 Figures 5b-d present a comparison of seasonally-averaged vertical O₃ profiles between the 1990s and the 2010s at
 318 the Naha, Tsukuba, and Sapporo sites. A parallel analysis is conducted for Hong Kong but for a comparison
 319 between the 2000s and 2010s (Figure 5a). While the general trend indicates an increase of O₃ mixing ratios with
 320 altitude, with higher values during spring and summer, several noteworthy features are identified from Figure 5.
 321 Firstly, vertical O₃ profiles vary with latitude and season. For instance, Hong Kong and Tsukuba show O₃ peaks
 322 within the ABL in autumn (black lines) and during summer (yellow lines), respectively. These peaks suggest a
 323 predominant influence of local anthropogenic emissions during the warmer months. A substantial O₃ peak at Hong
 324 Kong is observed around 0.2 normalized height (around 3-4 km above ground level) during spring. This
 325 enhancement is attributed to a combination of stratospheric intrusions and the transboundary transport of biomass-
 326 burning emissions originating from Southeast Asia (Liao et al., 2021; Zhao et al., 2021). On the other hand, Naha

327 and Sapporo do not exhibit discernible peaks in the lower troposphere, suggesting a relatively smaller impact from
 328 the combination of near-surface factors and stratospheric intrusions.

329
 330 Secondly, the seasonal minimum O₃ mixing ratios in the lower troposphere are observed during summer rather
 331 than winter, contrasting with the middle to upper troposphere observations over Hong Kong and Naha. This
 332 seasonal difference in the lower troposphere could be attributed to the influence of the East Asia Monsoon as
 333 discussed earlier. In the middle-upper troposphere, there are no such significant seasonal differences among sites.
 334 Conversely, the minimum seasonal O₃ mixing ratios occur during winter throughout the entire troposphere at the
 335 other two sites.

336
 337 Thirdly, enhancements of O₃ in the middle and upper troposphere are considerably more pronounced over Naha,
 338 Tsukuba, and Sapporo than over Hong Kong during the warm seasons (spring and summer) over the past three
 339 decades. This enhancement is particularly significant in the upper troposphere in Naha and Tsukuba during
 340 summer, as indicated by the dashed and solid yellow lines. In Hong Kong, enhancements are primarily observed
 341 at the top of the ABL in spring and within the ABL in fall, corresponding to where seasonal maxima are observed.
 342 These findings align with previous research (Huang et al., 2005; Ding et al., 2013; Liao et al., 2021; Lin et al.,
 343 2021).



344
 345 **Figure 5. A comparison of vertical profiles of seasonal mean O₃ during spring (red), summer (yellow), autumn (black),**
 346 **and winter (blue) at four sites (a) Hong Kong, (b) Naha, (c) Tsukuba, and (d) Sapporo between the first and the latest**
 347 **decades.**

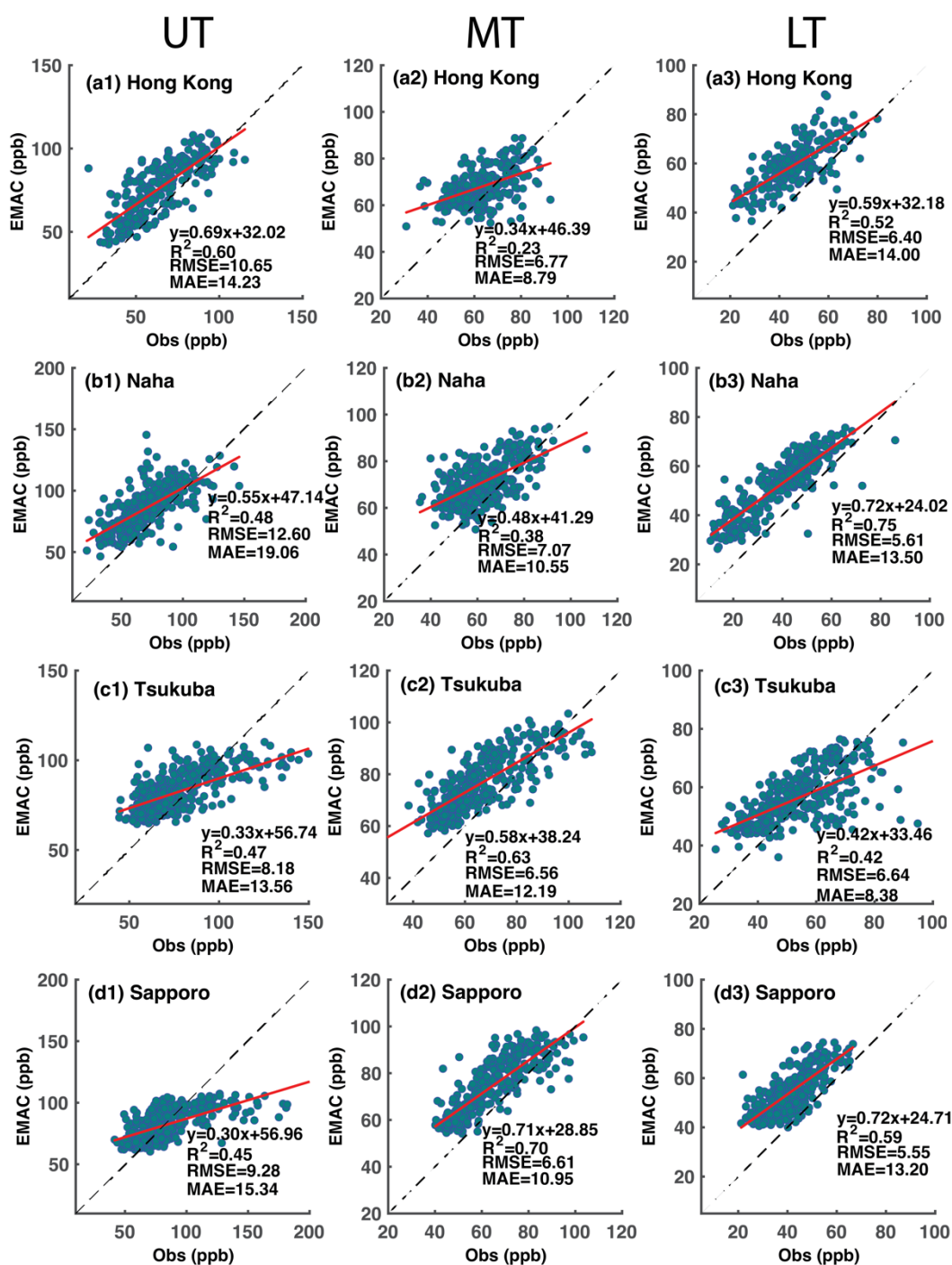
348
 349 **3.2 Comparison with observations and stratospheric versus tropospheric attribution using EMAC**
 350 **simulations**

351 In order to substantiate the observational findings, we now turn to the quantification of the relative contributions
 352 of key drivers to the observed changes in tropospheric O₃ based on the EMAC simulations.

353

354 3.2.1 Evaluation of EMAC simulations

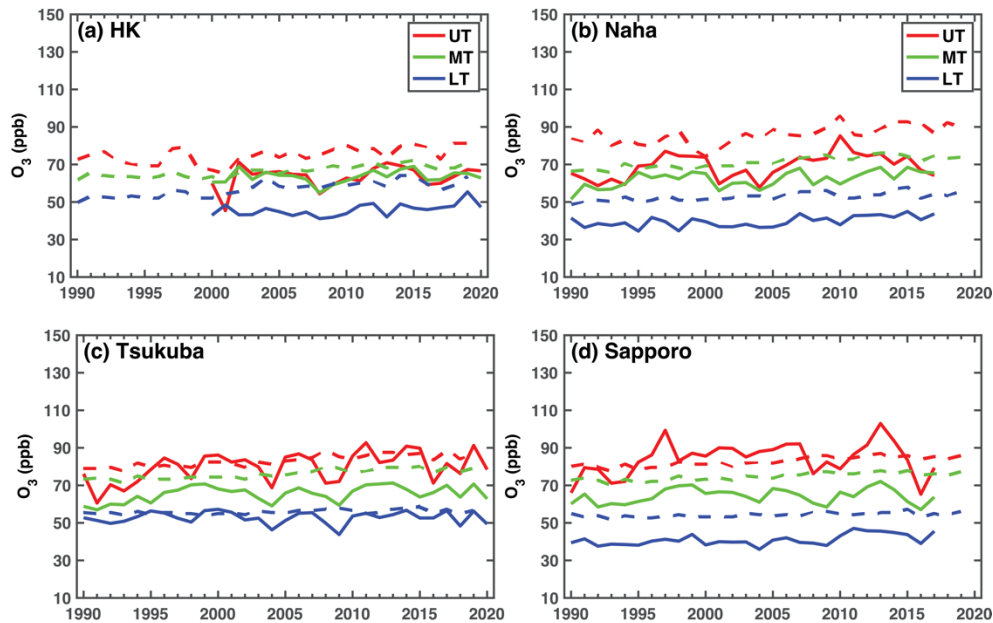
355 The EMAC simulations of O₃ for different altitude ranges in the troposphere are further evaluated with the O₃
356 sounding data during the study period. As illustrated in Figure 6, the majority of data points are located above the
357 1:1 line at all sites, indicating that the EMAC over-predicts O₃ in the troposphere, which agrees with other related
358 studies (Jöckel et al., 2016; Young et al., 2018; Revell et al 2018). The root mean standard error (RMSE) and mean
359 absolute error (MAE) of O₃ are generally larger in the UT than in MT and LT. The EMAC model shows a better
360 representation in the upper and lower troposphere than in the middle troposphere in Hong Kong and Naha, as
361 indicated by the coefficient of determinations (R²). For instance, R² reaches the highest value of 0.75 in the lower
362 troposphere over Naha (Figure 6b3), whereas R² is only about 0.23 for the middle troposphere over Hong Kong
363 (Figure 6a2). As for the mid-latitude sites, Tsukuba and Sapporo, the EMAC model shows a relatively good
364 representation of O₃ in the different layers of the troposphere, despite the overall overestimation, and in contrast
365 to the Hong Kong and Naha sites with highest R² in the MT. It is worth noting that although EMAC generally
366 overestimates O₃, there is a tendency towards higher overestimation for lower O₃ mixing ratios and lower
367 overestimation at higher O₃ mixing ratios, especially for the UT O₃ at the Tsukuba and Sapporo sites (Figure 6c1,
368 6d1).



369
 370 Figure 6 Evaluation of O₃ simulated with the EMAC model with observations in the upper troposphere (UT), middle
 371 troposphere (MT), and lower troposphere (LT) at the four sites: (a1-a3) Hong Kong, (b1-b3) Naha, (c1-c3)
 372 Tsukuba, and (d1-d3) Sapporo. The red lines are linear regression results between the observations and the EMAC model results.
 373 Black dash lines are 1:1 for reference. The statistical metrics including the coefficient of determinations (R²), root mean
 374 standard error (RMSE), and mean absolute error (MAE) are included for the quantitative evaluation of the model
 375 performance.

376
 377 Furthermore, the EMAC model predicts the realistic long-term trends of O₃ at different levels of the troposphere
 378 as indicated by the similar O₃ changes between monthly mean observation and model (Figure 7) as well as the
 379 comparable long-term change rates of model-predicted O₃ with the observations (Table 2). For example, the largest
 380 positive O₃ trends in the model also occur in the upper troposphere over Naha during summer at 0.75 ppb a⁻¹,

381 slightly less than the observations with 0.82 ppb a^{-1} for the past three decades (Table 2). Except for Hong Kong,
 382 the other three sites in the north have larger positive trends of O_3 in the upper troposphere than in the middle and
 383 lower troposphere from spring to autumn. Hong Kong shows a relatively large positive trend of O_3 in the middle
 384 and lower troposphere compared to other sites during the past 30 years.



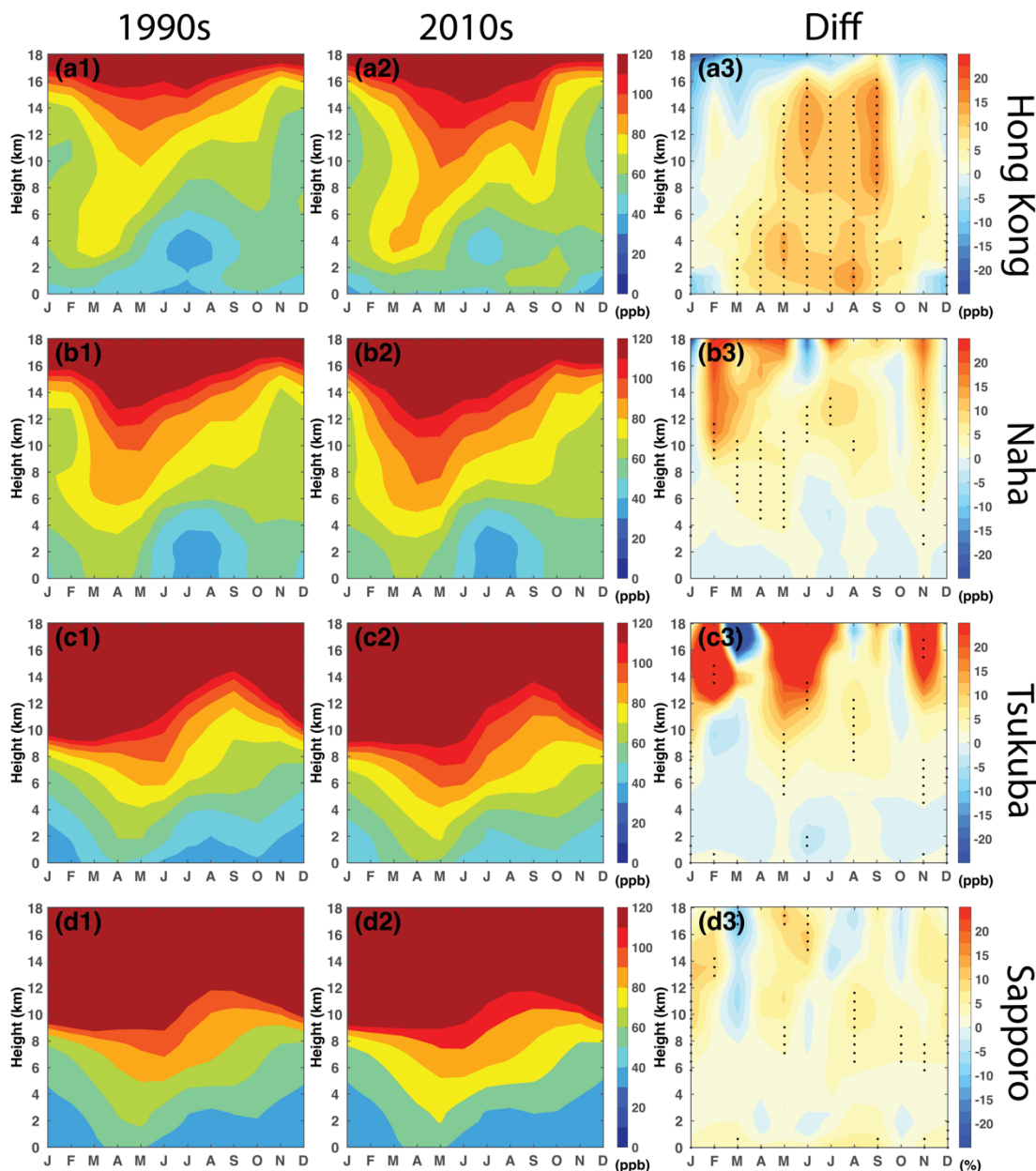
385
 386 Figure 7. Time series of monthly mean O_3 in ozonesonde (solid lines) and EMAC model (dash lines) for four sites at
 387 different layers of the troposphere.
 388

389 Table 2. The trends of EMAC-simulated O_3 (ppb a^{-1}) in the upper, middle, and lower troposphere in different seasons
 390 from 1990 to 2019. The observational O_3 trends are indicated in parentheses for comparison for the three Japanese
 391 sites. For the Hong Kong site, the O_3 trends since 2000 for both model (the first value) and observations (the second
 392 value) are in the square bracket. Note that observational periods for three Japanese sites are slightly different from the
 393 model (See Table 1). The trends with symbols (*) indicate the 95% confidence level. Bold indicates the agreement with
 394 the observations for significance and the sign of the trend. The trend with the same sign and both not significant are
 395 also indicated by bold. Normal font for the sign of the trend but not for significance, and italic for the opposite sign of
 396 the trend.

Station		MAM	JJA	SON	DJF
Hong Kong	UT	0.49* [0.98* 0.60*]	0.56* [0.49* −0.15]	0.32* [0.34 −0.14]	0.06 [0.25 −0.07]
	MT	0.33* [0.65* 0.20]	0.43* [0.39* −0.11]	0.36* [0.29 0.01]	0.01 [−0.01 0.27]
	LT	0.49* [0.65* 0.44*]	0.56* [0.53* 0.26]	0.32* [0.16 0.37]	0.06 [−0.18 0.16]
Naha	UT	0.33* (0.26)	0.75* (0.82*)	0.37* (0.21)	0.05 (0.06)
	MT	0.42* (0.41*)	0.33* (0.44*)	0.33* (0.31*)	0.10* (0.02)
	LT	0.32* (0.38*)	0.21* (0.23*)	0.09 (0.13)	0.08* (0.14*)
Tsukuba	UT	0.26* (0.63*)	0.45* (0.67*)	0.32* (0.31*)	0.12 (−0.05)
	MT	0.21* (0.17)	0.37* (0.42*)	0.28* (0.29*)	0.14* (0.03)
	LT	0.13*(0.11)	0.09 (−0.20)	0.03 (0.01)	0.05* (0.13*)
Sapporo	UT	0.22* (0.26)	0.34* (0.68)	0.25* (0.13)	0.15* (0.07)
	MT	0.18* (0.12)	0.28* (0.14)	0.21* (0.04)	0.11* (0.06)
	LT	0.12* (0.29*)	0.12* (0.05)	0.03 (0.13)	0.03 (0.31*)

397
 398 Figure 8 demonstrates the month-height cross-sections of EMAC-predicted monthly-mean O_3 and their changes
 399 in the troposphere at the four sites between the 1990s and 2010s. Compared with the observed counterparts (Figure
 400 4), the model reproduces the temporal-spatial variation patterns of tropospheric O_3 within the troposphere

401 quantitatively well. Specifically, the model captures a key feature with the O₃ tongue that occurs from late spring
 402 to early summer over four sites and their variation with latitude. The summer relatively "clean" layer with low O₃
 403 mixing ratios in the lower troposphere at the southern sites of Hong Kong and Naha is also well simulated.



404
 405 **Figure 8.** EMAC-simulated monthly mean O₃ in the 1990s and 2010s, and their differences between 2010s and 1990s at
 406 the four observation sites (a1-a3) Hong Kong, (b1-b3) Naha, (c1-c3) Tsukuba and (d1-d3) Sapporo. The horizontal axes
 407 denote the months of the year and the vertical axes represent the height above ground. Dots in the a3-d3 represent the
 408 layer with statistically significant changes according to a paired two-sided t-test ($p < 0.05$).
 409

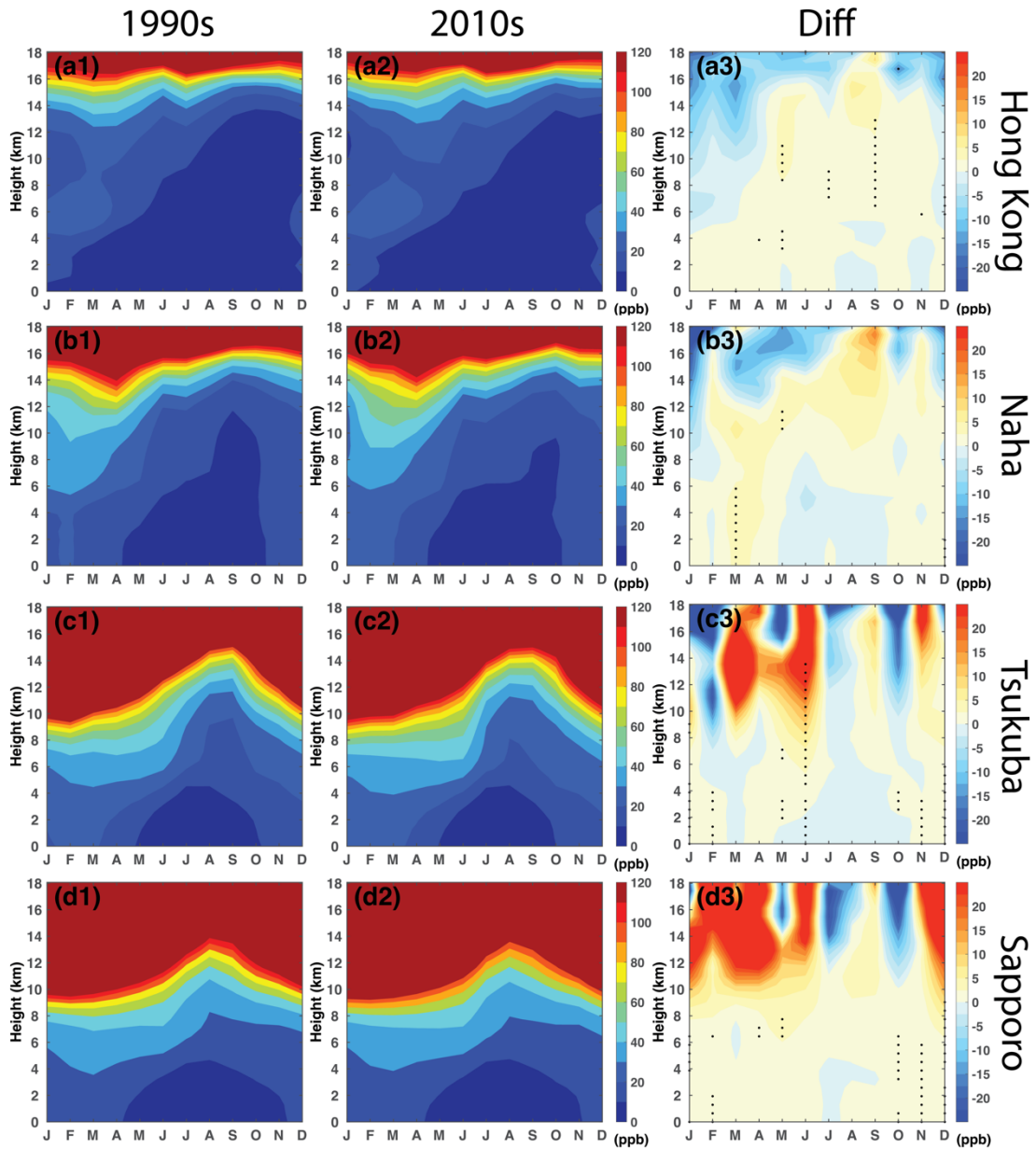
410 Overall, the EMAC model reasonably simulates the spatial and temporal variations in tropospheric O₃ as compared
 411 to the O₃ observations at the four sounding sites. Consistency between the model and observations suggests that
 412 the trends observed in the Japanese ozonesondes remain valuable despite uncertainties related to the transitions
 413 between the two types of ozonesondes. Moreover, the model can effectively be used to investigate the drivers of
 414 these trends.
 415

416 3.2.2 Changes in O₃S and O₃T derived from EMAC simulations

417 To gain deeper insights into the factors contributing to tropospheric O₃, we analyze the EMAC-simulated total O₃
418 in the troposphere, origin of O₃ from the stratosphere (i.e., stratospheric intrusion, O₃S), and origin of O₃ from the
419 troposphere (i.e., photochemical production in the troposphere, O₃T) at the four sites, along with their latitudinal
420 variations (Figures 9 and 10). The layer with the large mixing ratio of O₃S extending from the lower stratosphere
421 to the troposphere occurs in early spring at the southern site (i.e., Hong Kong). Conversely, similar occurrences
422 are observed to shift to early summer in the northern site (i.e., Sapporo) (Figure 9). The seasonal buildup of mid-
423 latitude total O₃ typically unfolds from winter through late spring, followed by a decline in summer (Fioletov and
424 Shepherd, 2003). The seasonal lifting of the tropopause will naturally contribute to the entrainment of O₃-rich air
425 from the stratosphere into the troposphere (Monks, 2000). Furthermore, together with dynamical processes such
426 as tropopause folding in the vicinity of the subtropical jet (Baray et al., 2000), stratospheric O₃ is transported
427 downward into the troposphere. Over the past 30 years, the two sites within the subtropics (Tsukuba at 36°N and
428 Sapporo at 43°N) exhibit larger O₃S increases in the lower stratosphere and upper troposphere compared to the
429 other two sites situated in the near-tropical region (Hong Kong at 22°N and Naha at 26°N).

430
431 The O₃T shows seasonal maxima during the warm seasons (from March to October) throughout the troposphere
432 in Hong Kong, while mainly occurring in the middle to upper troposphere among three Japan sites (Figure 10). In
433 the lower troposphere at Hong Kong, the O₃T contributes more than O₃S (60-80 ppb vs. 10-20 ppb) in the separated
434 O₃ hotspots around 2-4 km during spring. In the tropical regions, air rises in the Hadley cell from the surface to
435 the upper troposphere, and further ascent into the stratosphere where it is transported to the mid-latitudes by the
436 BDC (Brewer, 1949; A. Stohl et al., 2003). In this way, the tropospheric origin O₃ could be further transported to
437 the middle-upper troposphere of middle-latitude regions.

438
439 Several factors influence O₃ mixing ratios over study regions, which could potentially be responsible for the local
440 maxima in O₃T: transport from near-surface tropospheric O₃ within the upward branch of the Hadley cell into the
441 upper troposphere; horizontal transport from upstream polluted regions, e.g., mainland China in this study;
442 biomass burning related transport; enhanced mixture by active convection and lightning events; local photochemical
443 O₃ production. O₃T has shown significant enhancements among the four sites over the past several decades.
444 However, the primary contributors to the high O₃T concentrations and their enhancement vary with locations and
445 layers, which require further investigation.



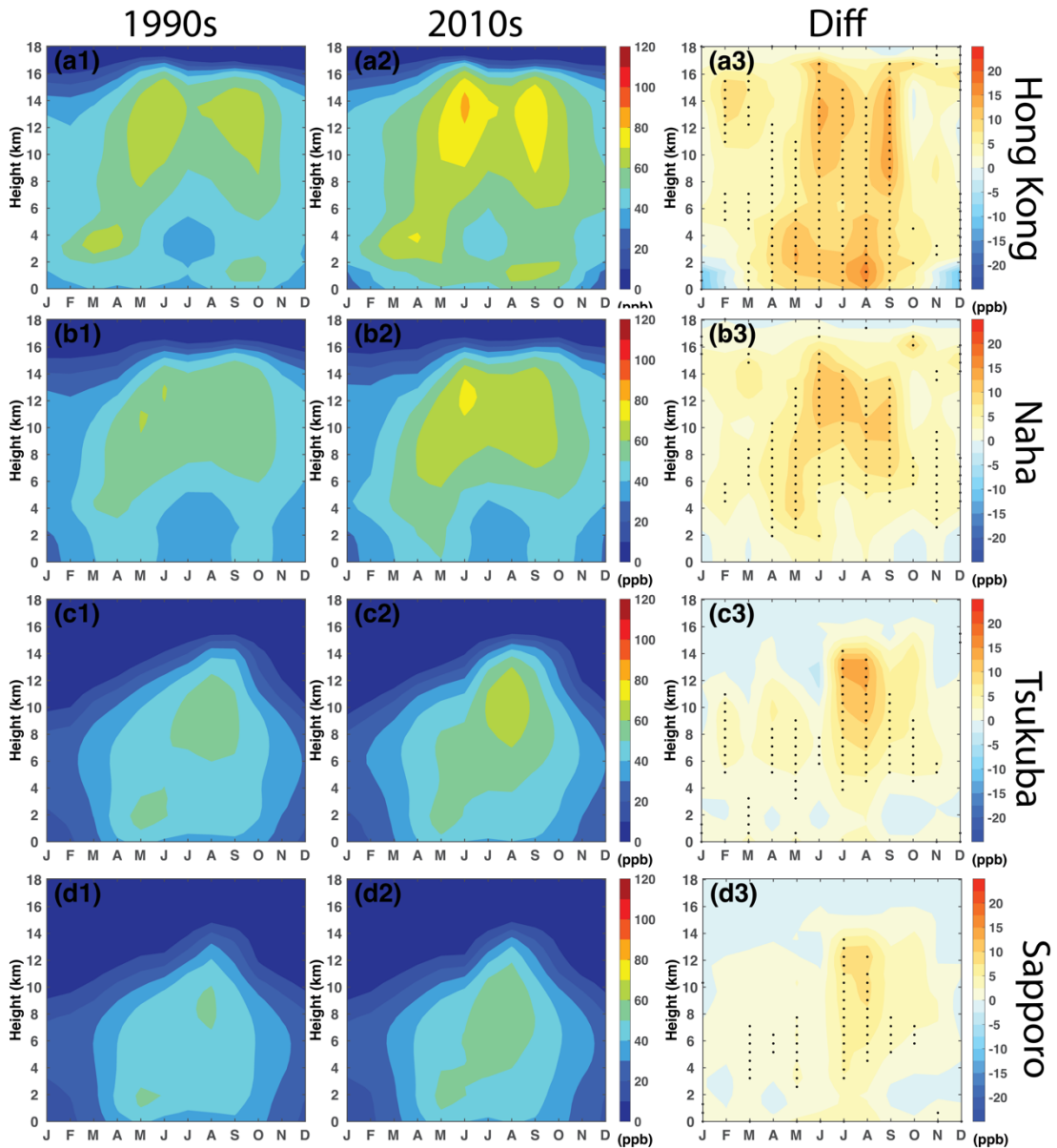
446

447

448

449

Figure 9. A comparison of the EMAC-simulated monthly mean temporal and spatial distributions of O₃S in the 1990s and 2010s, and the difference between 2010s and 1990s at the four observation sites: Hong Kong, Naha, Tsukuba, and Sapporo. Dots represent the layer with statistically significant changes according to a paired two-sided t-test ($p < 0.05$).



450
451 **Figure 10. Similar to Figure 9 but for the component of tropospheric O₃ (O₃T).**

452

453 **3.2.3 Attribution of EMAC tropospheric O₃ changes: O₃S vs. O₃T**

454 Utilizing the reasonably realistic simulations of tropospheric O₃ and their variations by the EMAC model, we can
 455 now quantify the respective contributions of O₃S and O₃T to the changes in tropospheric O₃ between the 2010s
 456 and 1990s, as presented in Table 3. Overall, the increase of O₃T (up to 11.09 ppb) dominates the O₃ increase
 457 throughout the troposphere at all the sites during summer. Particularly for the near-tropical sites, Hong Kong and
 458 Naha, the increase of O₃T contributes more than the O₃S changes with percentage contributions greatly more than
 459 60%, even offsetting the decrease in O₃S during winter and spring. Conversely, for the subtropical sites, Tsukuba
 460 and Sapporo, O₃S emerges as the primary driver for changes in the middle-upper tropospheric O₃ during winter
 461 and spring. The contribution of O₃S to observed O₃ increases by up to 96% at Sapporo in DJF and 40% at Tsukuba
 462 in JJA in the upper troposphere (Table 3)

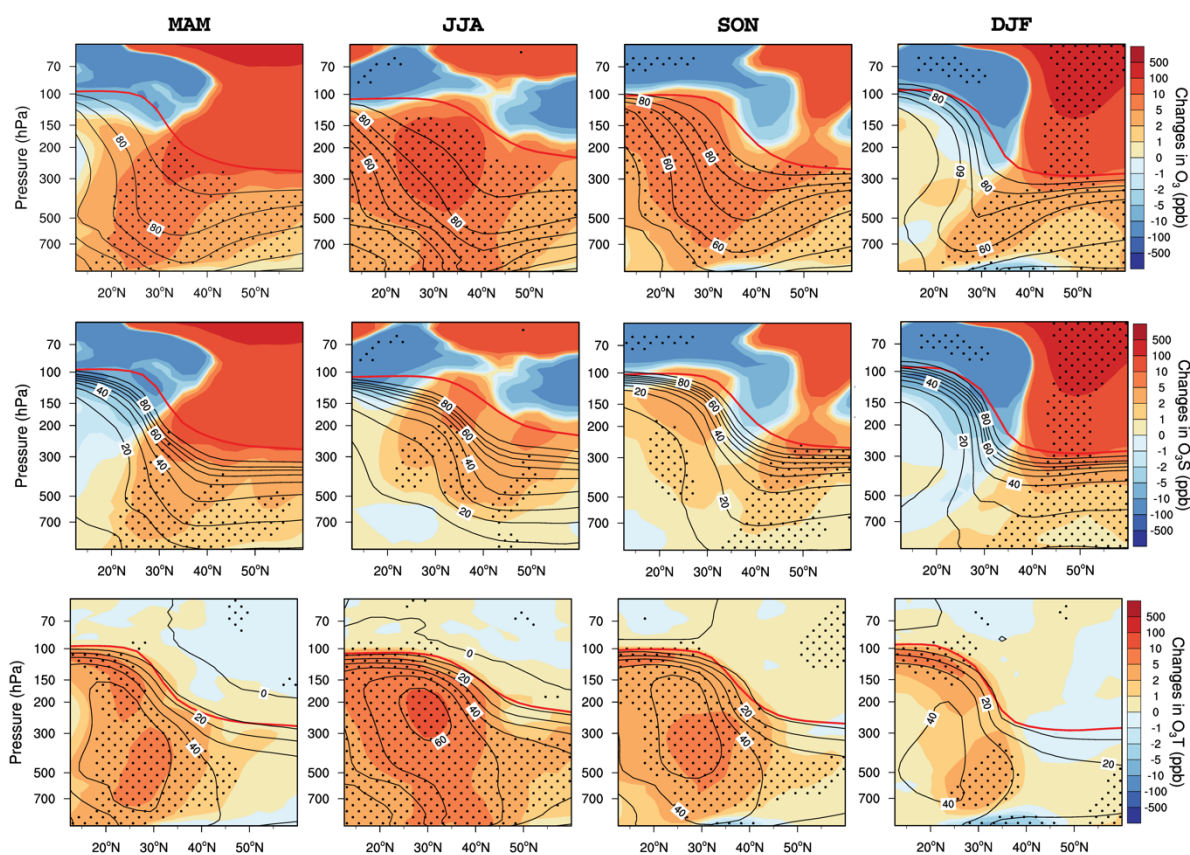
463 Table 3. Tropospheric O₃ changes and contributions from O₃S and O₃T to changes of tropospheric O₃ between the 2010s and 1990s at the upper, middle, and lower troposphere (UT, MT,
 464 and LT) in different seasons. The percentage contributions of O₃S and O₃T to O₃ changes are listed in the parentheses.
 465

Station		O ₃ changes (ppb)				O ₃ S changes (ppb)				O ₃ T changes (ppb)			
		MAM	JJA	SON	DJF	MAM	JJA	SON	DJF	MAM	JJA	SON	DJF
Hong Kong	UT	3.55	12.53	7.09	-0.40	-2.03 (-57%)	1.44 (11%)	1.41 (20%)	-3.44 (860%)	5.58 (157%)	11.09 (89%)	5.69 (80%)	3.04 (-760%)
	MT	6.35	9.22	7.50	0.32	1.30 (20%)	0.96 (10%)	1.23 (16%)	-2.84 (-888%)	5.06 (80%)	8.27 (90%)	6.27 (84%)	3.16 (988%)
	LT	9.62	11.47	6.28	2.10	0.88 (9%)	0.10 (1%)	-0.13 (-2%)	1.24 (59%)	8.73 (91%)	11.37 (99%)	6.41 (102%)	0.86 (41%)
Naha	UT	5.94	14.76	7.76	1.31	1.05 (18%)	3.81(26%)	2.98 (38%)	-1.87 (-143%)	4.90 (82%)	10.95 (74%)	4.78 (62%)	3.18 (243%)
	MT	8.52	6.29	6.74	2.19	2.32 (27%)	0.08 (1%)	1.10 (16%)	-1.03 (-47%)	6.19 (73%)	6.22 (99%)	5.64 (84%)	3.22 (147%)
	LT	5.86	3.32	1.75	1.71	2.35 (40%)	-0.19 (-6%)	0.07 (4%)	0.73 (43%)	3.51 (60%)	3.51 (106%)	1.68 (96%)	0.98 (57%)
Tsukuba	UT	10.65	11.45	6.35	-2.08	7.33 (69%)	4.23 (40%)	2.19 (34%)	-4.59 (221%)	3.32 (31%)	7.22 (60%)	4.15 (66%)	2.51 (-121%)
	MT	4.54	7.39	5.18	2.74	1.50 (33%)	2.10 (28%)	1.39 (27%)	0.51 (19%)	3.04 (67%)	5.29 (72%)	3.79 (73%)	2.23 (81%)
	LT	2.50	2.17	0.24	0.98	1.27 (51%)	0.44 (20%)	0.94 (392%)	0.90 (92%)	1.22 (49%)	1.74 (80%)	-0.70 (-292%)	0.08 (8%)
Sapporo	UT	8.66	8.58	5.11	4.82	6.85 (79%)	3.19 (37%)	2.00 (39%)	4.65 (96%)	1.82 (21%)	5.40 (63%)	3.11 (61%)	0.17 (4%)
	MT	3.80	5.73	3.88	2.27	1.60 (42%)	1.59 (28%)	1.31 (34%)	1.62 (71%)	2.20 (58%)	4.14 (72%)	2.57 (66%)	0.65 (29%)
	LT	2.37	2.80	0.27	0.60	1.19 (50%)	0.35 (13%)	0.71 (263%)	0.69 (115%)	1.18 (50%)	2.45 (87%)	-0.45 (-163%)	-0.09 (-15%)

466 To get a more complete picture of how tropospheric O₃ changes along the Northwest Pacific regions, the zonal
 467 mean of tropospheric O₃, O₃S, and O₃T changes are compared in Figure 11 and Figure S6. The climatological
 468 distribution of vertical tropospheric O₃ with latitude is determined by O₃S in the subtropics and O₃T in the tropics.
 469

470 Tropospheric O₃ shows statistically significant positive changes from 10°N to 60°N in summer, with the maximum
 471 in the middle to upper troposphere around 30°N. Similarly, O₃T demonstrates a similar pattern of changes as
 472 tropospheric O₃ in summer, indicating that tropospheric photochemical O₃ production is the primary driver of the
 473 summertime tropospheric O₃ enhancement. Strengthened downward transport of stratospheric O₃ primarily affects
 474 the upper troposphere in the subtropics during summer.

475
 476 Conversely, during winter and spring, the O₃S significantly contributes to the enhancement of tropospheric O₃ in
 477 the subtropics. Positive changes in O₃T are observed south of 40°N, partly offsetting the decrease in O₃S in the
 478 upper troposphere.



479
 480 **Figure 11. Latitude-pressure cross sections of mixing ratio difference of O₃, O₃S, and O₃T (ppb) between the 2010s and**
 481 **1990s along the Northwest Pacific region (zonal mean over 110°E to 150°E) in four seasons. Black lines indicate the**
 482 **climatological distribution. Red solid lines denote the tropopause height. Dots represent the layer with statistically**
 483 **significant changes according to a paired two-sided t-test ($p < 0.05$).**
 484

485 4. Discussion and Conclusion

486 In this study, thirty years of ozonesonde observational data at four ozonesonde sites (Hong Kong, Naha, Tsukuba,
 487 and Sapporo) are presented together with simulation results of the chemistry-climate model EMAC to characterize

488 the temporal and spatial variation patterns and the long-term changes of tropospheric O₃ along the Northwest
489 Pacific region.

490

491 The analysis of the seasonality in O₃ shows a seasonal maximum throughout the troposphere, occurring in late
492 spring at the tropical site Hong Kong and shifting to early summer at the mid-latitude sites such as Sapporo.
493 Additionally, for Hong Kong and Naha, the lower tropospheric O₃ exhibits a seasonal minimum. As for long-term
494 changes, tropospheric O₃ generally increases at all four sites. Naha and Tsukuba, show larger positive trends of
495 O₃ up to 0.82 ppb a⁻¹, particularly in the upper and middle troposphere. The aggregation analysis between different
496 decades indicates that the seasonal maximum in the troposphere becomes more pronounced and deeper over time.

497

498 Based on EMAC simulations, the summer and autumn enhancement of O₃ in the middle-upper troposphere is
499 mostly attributable to tropospheric O₃ source linked to increasing pollution emissions, with percentage
500 contributions more than 60%. On the other hand, O₃ originating from the stratosphere dominates the large portion
501 of middle-upper tropospheric O₃ enhancement by 19-96% and 28-40% in the mid-latitude during winter and
502 spring. The climatological maximum observed in the seasonality of O₃ throughout the troposphere is associated
503 with both stratosphere-troposphere exchange north of 30°N and photochemical O₃ production in the troposphere
504 in spring. These findings corroborate the features discussed by Oltmans et al. (2004), confirming them with a
505 longer observational dataset based on the tagged O₃ tracers in the EMAC model. Our results further confirm the
506 offsetting effect of O₃T increase to the decrease in O₃S in the tropical troposphere during winter and spring.

507

508 While the magnitude of O₃ trends is well simulated with the EMAC model in most atmospheric layers,
509 uncertainties persist in the mean values due to various factors. These include large dynamical variability
510 perturbing stratosphere-to-troposphere O₃ transport, the influence of O₃-depleting substances, uncertainties of
511 long-term changes in emissions, insufficient treatment of chemical processes, or inaccurate transport due to
512 excessive numerical diffusion in the tropopause region, etc. Additionally, uncertainties may arise from
513 interpolating the relatively coarse horizontal and vertical resolution of the global model data to the locations of the
514 observational sites. Nevertheless, the presented results indicate a satisfactory level of agreement between the
515 model results and the observations, allowing further disentangling of O₃T versus O₃S contributions.

516

517 The dynamical and chemical drivers for such long-term tropospheric changes deserve further analysis in the future.
518 Here, we propose several mechanisms based on related research that could potentially contribute to observed
519 tropospheric O₃ enhancements in East Asia. Regional transport is one important contributor to tropospheric O₃
520 enhancement. Compared with the other two Japanese sites, Naha, to the east of China, is susceptible to regional
521 transport of air pollution from China. The prevailing westerly winds bring O₃-enriched air from eastern China to
522 Naha, resulting in a substantial increase of O₃ from the middle to upper troposphere. Internal dynamical
523 variabilities such as the warm phase of El Niño-Southern Oscillation (ENSO) and the easterly phase of the Quasi-
524 Biennial Oscillation (QBO) are known to be closely tied to enhanced STT of O₃ (Neu et al 2014, Zeng and Pyle,
525 2005). The ENSO/QBO-related changes can influence jet stream variations, leading to the formation of tropopause
526 folds through Rossby wave breaking (Albers et al 2018). Increased frequency and the northward shift of tropopause
527 folding events are observed in the East Asia region (Figure S7), attributed to an increase in the zonal wind and
528 poleward-upward shift of the STJ driven by global warming-induced increases in greenhouse gasses (Akritidis et

529 al 2019, Manney and Hegglin, 2018). With increasing greenhouse gases, the BDC tends to strengthen due to larger
530 zonal-mean temperature gradients and increased wave drag in the extratropical stratosphere (Shepherd and
531 McLandress, 2011; Neu et al 2014). This results in an increased O₃ reservoir over the subtropical LMS, facilitating
532 downward transport to the troposphere under the influence of the Pacific jet (Hegglin and Shepherd, 2009; Albers
533 et al 2018).

534

535 **Data Availability Statement:** The ozone-sounding dataset used for observational analysis in the study is publicly
536 available at the World Ozone and Ultraviolet Radiation Data Centre via
537 <https://woudc.org/data/explore.php?lang=en> (last access: 25 Feb 2024). The EMAC model output used in the paper
538 has been published on Zenodo, which can be freely downloaded via <https://zenodo.org/records/11093806>.

539 **Supplement:** Supplementary.pdf

540

541 **Author Contributions:** XM carried out all the observational and model simulation data analyses, led the
542 interpretation of the results, and prepared the manuscript with contributions from all the co-authors. JH, MH, PJ,
543 and TZ contributed to the interpretation of the results and provided extensive comments on the manuscript. PJ
544 conducted the EMAC simulations.

545

546 **Competing interests:** At least one of the (co-)authors is a member of the editorial board of Atmospheric Chemistry
547 and Physics.

548

549 **Acknowledgment:** This research has been supported by the National Key Research and Development Program
550 of China (2022YFC3701204), the National Natural Science Foundation of China (42275196, 42105164), and the
551 Applied Basic Research Foundation (2022A1515011078). The EMAC simulations have been performed at the
552 German Climate Computing Centre (DKRZ) through support from the Bundesministerium für Bildung und
553 Forschung (BMBF). DKRZ and its scientific steering committee are gratefully acknowledged for providing the
554 HPC and data archiving resources for this consortial project ESCiMo (Earth System Chemistry integrated
555 Modelling). We especially thank Michael Sprenger from ETH Zurich for providing the tropopause folding
556 frequency dataset. We also thank four anonymous reviewers and Kaihui Zhao for providing comments on the
557 initial submission of this paper.

558

559 **References**

560 Akritidis, D., Pozzer, A., and Zanis, P.: On the impact of future climate change on tropopause folds and
561 tropospheric ozone, *Atmos. Chem. Phys.*, 19, 14387-14401, <https://doi.org/10.5194/acp-19-14387-2019>, 2019.

562 Albers, J. R., Perlwitz, J., Butler, A. H., Birner, T., Kiladis, G. N., Lawrence, Z. D., Manney, G. L., Langford, A.
563 O., and Dias, J.: Mechanisms governing interannual variability of stratosphere-to-troposphere ozone transport, *J.*
564 *Geophys. Res.*, 123, 234-260, <https://doi.org/10.1002/2017JD026890>, 2018.

565 Bak, J., Baek, K. H., Kim, J. H., Liu, X., Kim, J., and Chance, K.: Cross-evaluation of GEMS tropospheric ozone
566 retrieval performance using OMI data and the use of an ozonesonde dataset over East Asia for validation, *Atmos.*
567 *Meas. Tech.*, 12, 5201-5215, <https://doi.org/10.5194/amt-12-5201-2019>, 2019.

568 Baray, J.-L., Daniel, V., Ancellet, G., and Legras, B.: Planetary-scale tropopause folds in the southern subtropics,
569 *Geophys. Res. Lett.*, 27, 353-356, <https://doi.org/10.1029/1999GL010788>, 2000.

570 Birner, T., and Bönisch, H.: Residual circulation trajectories and transit times into the extratropical lowermost
571 stratosphere, *Atmos. Chem. Phys.*, 11, 817-827, <https://doi.org/10.5194/acp-11-817-2011>, 2011.

572 Bönisch, H., Engel, A., Curtius, J., Birner, T., and Hoor, P.: Quantifying transport into the lowermost stratosphere
573 using simultaneous in-situ measurements of SF₆ and CO₂, *Atmos. Chem. Phys.*, 9, 5905-5919,
574 <https://doi.org/10.5194/acp-9-5905-2009>, 2009.

575 Brewer, A. W.: Evidence for a world circulation provided by the measurements of helium and water vapour
576 distribution in the stratosphere, *Q. J. Roy. Meteor. Soc.*, 75, 351-363, <https://doi.org/10.1002/qj.49707532603>,
577 1949.

578 Chang, K.-L., Petropavlovskikh, I., Cooper, O. R., Schultz, M. G., and Wang, T.: Regional trend analysis of surface
579 ozone observations from monitoring networks in eastern North America, Europe and East Asia, *Elem. Sci. Anth.*,
580 5, <https://doi.org/10.1525/elementa.243>, 2017.

581 Collins, J. W.: Effect of stratosphere-troposphere exchange on the future tropospheric ozone trend, *J. Geophys.*
582 *Res.*, 108, <https://doi.org/10.1029/2002JD002617>, 2003.

583 Cooper, O. R., Parrish, D. D., Ziemke, J., Balashov, N. V., Cupeiro, M., Galbally, I. E., Gilge, S., Horowitz, L.,
584 Jensen, N. R., Lamarque, J.-F., Naik, V., Oltmans, S. J., Schwab, J., Shindell, D. T., Thompson, A. M., Thouret,
585 V., Wang, Y., and Zbinden, R. M.: Global distribution and trends of tropospheric ozone: An observation-based
586 review, *Elem. Sci. Anth.*, 2, <https://doi.org/10.12952/journal.elementa.000029>, 2014.

587 Ding, A. J., and Wang, T.: Influence of stratosphere-to-troposphere exchange on the seasonal cycle of surface
588 ozone at Mount Waliguan in western China, *Geophys. Res. Lett.*, 33, L03803,
589 <https://doi.org/10.1029/2005GL024760>, 2006.

590 Ding, A. J., Wang, T., and Fu, C. B.: Transport characteristics and origins of carbon monoxide and ozone in Hong
591 Kong, South China, *J. Geophys. Res.*, 118, 9475-9488, <https://doi.org/10.1002/jgrd.50714>, 2013.

592 Duncan, B. N., Lamsal, L. N., Thompson, A. M., Yoshida, Y., Lu, Z., Streets, D. G., Hurwitz, M. M., and
593 Pickering, K. E.: A space-based, high-resolution view of notable changes in urban NO_x pollution around the world
594 (2005–2014), *J. Geophys. Res.*, 121, 976-996, <https://doi.org/10.1002/2015JD024121>, 2016.

595 Fioletov, V. E., and Shepherd, T. G.: Seasonal persistence of midlatitude total ozone anomalies, *Geophys. Res.*
596 *Lett.*, 30, <https://doi.org/10.1029/2002GL016739>, 2003.

597 Granier, C., Bessagnet, B., Bond, T., D'Angiola, A., Denier van der Gon, H., Frost, G. J., Heil, A., Kaiser, J. W.,
598 Kinne, S., Klimont, Z., Kloster, S., Lamarque, J.-F., Liousse, C., Masui, T., Meleux, F., Mieville, A., Ohara, T.,
599 Raut, J.-C., Riahi, K., Schultz, M. G., Smith, S. J., Thompson, A., van Aardenne, J., van der Werf, G. R., and van
600 Vuuren, D. P.: Evolution of anthropogenic and biomass burning emissions of air pollutants at global and regional
601 scales during the 1980–2010 period, *Clim. Change.*, 109, 163, <https://doi.org/10.1007/s10584-011-0154-1>, 2011.

602 Griffiths, P. T., Keeble, J., Shin, Y. M., Abraham, N. L., Archibald, A. T., and Pyle, J. A.: On the Changing Role
603 of the Stratosphere on the Tropospheric Ozone Budget: 1979–2010, *Geophys. Res. Lett.*, 47, e2019GL086901,
604 <https://doi.org/10.1029/2019GL086901>, 2020.

605 Hegglin, M. I., and Shepherd, T. G.: O₃-N₂O correlations from the Atmospheric Chemistry Experiment:
606 Revisiting a diagnostic of transport and chemistry in the stratosphere, *J. Geophys. Res. Atmos.*, 112,
607 <https://doi.org/10.1029/2006JD008281>, 2007.

608 Hegglin, M. I., and Shepherd, T. G.: Large climate-induced changes in ultraviolet index and stratosphere-to-
609 troposphere ozone flux, *Nat. Geosci.*, 2, 687-691, <https://doi.org/10.1038/ngeo604>, 2009.

610 Hersbach, H., Bell, B., Berrisford, P., Hirahara, S., Horányi, A., Muñoz-Sabater, J., Nicolas, J., Peubey, C., Radu,
611 R., Schepers, D., Simmons, A., Soci, C., Abdalla, S., Abellan, X., Balsamo, G., Bechtold, P., Biavati, G., Bidlot,
612 J., Bonavita, M., De Chiara, G., Dahlgren, P., Dee, D., Diamantakis, M., Dragani, R., Flemming, J., Forbes, R.,
613 Fuentes, M., Geer, A., Haimberger, L., Healy, S., Hogan, R. J., Hólm, E., Janisková, M., Keeley, S., Laloyaux, P.,
614 Lopez, P., Lupu, C., Radnoti, G., de Rosnay, P., Rozum, I., Vamborg, F., Villaume, S., and Thépaut, J.-N.: The
615 ERA5 global reanalysis, *Q. J. R. Meteorol. Soc.*, 146, 1999-2049, <https://doi.org/10.1002/qj.3803>, 2020.

616 Holton, J. R., Haynes, P. H., McIntyre, M. E., Douglass, A. R., Rood, R. B., and Pfister, L.: Stratosphere-
617 troposphere exchange, *Rev. Geophys.*, 33, 403-439, <https://doi.org/10.1029/95RG02097>, 1995.

618 Huang, J. P., Fung, J. C., Lau, A. K., and Qin, Y.: Numerical simulation and process analysis of typhoon-related
619 ozone episodes in Hong Kong, *J. Geophys. Res.*, 110, <https://doi.org/10.1029/2004JD004914>, 2005.

620 Jöckel, P., Tost, H., Pozzer, A., Brühl, C., Buchholz, J., Ganzeveld, L., Hoor, P., Kerkweg, A., Lawrence, M. G.,
621 Sander, R., Steil, B., Stiller, G., Tanarhte, M., Taraborrelli, D., van Aardenne, J., and Lelieveld, J.: The atmospheric
622 chemistry general circulation model ECHAM5/MESy1: consistent simulation of ozone from the surface to the
623 mesosphere, *Atmos. Chem. Phys.*, 6, 5067-5104, <https://doi.org/10.5194/acp-6-5067-2006>, 2006.

624 Jöckel, P., Tost, H., Pozzer, A., Kunze, M., Kirner, O., Brenninkmeijer, C. A. M., Brinkop, S., Cai, D. S., Dyroff,
625 C., Eckstein, J., Frank, F., Garny, H., Gottschaldt, K. D., Graf, P., Grewe, V., Kerkweg, A., Kern, B., Matthes, S.,

- 626 Mertens, M., Meul, S., Neumaier, M., Nützel, M., Oberländer-Hayn, S., Ruhnke, R., Runde, T., Sander, R.,
627 Scharffe, D., and Zahn, A.: Earth System Chemistry integrated Modelling (ESCiMo) with the Modular Earth
628 Submodel System (MESSy) version 2.51, *Geosci. Model Dev.*, 9, 1153-1200, [https://doi.org/10.5194/gmd-9-](https://doi.org/10.5194/gmd-9-1153-2016)
629 1153-2016, 2016.
- 630 Jöckel, P., Brinkop, S., Graf, P., Eichinger, R., Garny, H., Mertens, M., Nützel, M., and Pozzer, A.: RD1SD:
631 EMAC CCM1-2022 hindcast simulations with specified dynamics, ERA-5, 1979-2019 (additional data), in,
632 DOKU at DKRZ, 2024a.
- 633 Jöckel, P., Brinkop, S., Graf, P., Eichinger, R., Garny, H., Mertens, M., Nützel, M., Pozzer, A., Tost, H., and The,
634 M. C.: RD1SD: EMAC CCM1-2022 hindcast simulations with specified dynamics, ERA-5, 1979-2019, in, World
635 Data Center for Climate (WDCC) at DKRZ, 2024b.
- 636 Johnson, B. J., Oltmans, S. J., Vömel, H., Smit, H. G. J., Deshler, T., and Kröger, C.: Electrochemical
637 concentration cell (ECC) ozonesonde pump efficiency measurements and tests on the sensitivity to ozone of
638 buffered and unbuffered ECC sensor cathode solutions, *J. Geophys. Res.*, 107, ACH 8-1-ACH 8-18,
639 <https://doi.org/10.1029/2001JD000557>, 2002.
- 640 Kerkweg, A., Sander, R., Tost, H., and Jöckel, P.: Technical note: Implementation of prescribed (OFFLEM),
641 calculated (ONLEM), and pseudo-emissions (TNUDGE) of chemical species in the Modular Earth Submodel
642 System (MESSy), *Atmos. Chem. Phys.*, 6, 3603-3609, <https://doi.org/10.5194/acp-6-3603-2006>, 2006.
- 643 Konopka, P., Ploeger, F., Tao, M., Birner, T., and Riese, M.: Hemispheric asymmetries and seasonality of mean
644 age of air in the lower stratosphere: Deep versus shallow branch of the Brewer-Dobson circulation, *J. Geophys.*
645 *Res. Atmos.*, 120, 2053-2066, <https://doi.org/10.1002/2014JD022429>, 2015.
- 646 Krotkov, N. A., McLinden, C. A., Li, C., Lamsal, L. N., Celarier, E. A., Marchenko, S. V., Swartz, W. H., Bucsela,
647 E. J., Joiner, J., Duncan, B. N., Boersma, K. F., Veefkind, J. P., Levelt, P. F., Fioletov, V. E., Dickerson, R. R.,
648 He, H., Lu, Z., and Streets, D. G.: Aura OMI observations of regional SO₂ and NO₂ pollution changes from 2005
649 to 2015, *Atmos. Chem. Phys.*, 16, 4605-4629, <https://doi.org/10.5194/acp-16-4605-2016>, 2016.
- 650 Kunze, M., Godolt, M., Langematz, U., Grenfell, J. L., Hamann-Reinus, A., and Rauer, H.: Investigating the early
651 Earth faint young Sun problem with a general circulation model, *Planet. Space Sci.*, 98, 77-92,
652 <https://doi.org/10.1016/j.pss.2013.09.011>, 2014.
- 653 Li, K., Jacob, D. J., Liao, H., Shen, L., Zhang, Q., and Bates, K. H.: Anthropogenic drivers of 2013–2017 trends
654 in summer surface ozone in China, *P. Natl. Acad. Sci.*, 116, 422-427, <https://doi.org/10.1073/pnas.1812168116>
655 2019.
- 656 Liao, Z., Ling, Z., Gao, M., Sun, J., Zhao, W., Ma, P., Quan, J., and Fan, S.: Tropospheric Ozone Variability Over
657 Hong Kong Based on Recent 20 years (2000–2019) Ozonesonde Observation, *J. Geophys. Res.*, 126,
658 e2020JD033054, <https://doi.org/10.1029/2020JD033054>, 2021.
- 659 Lin, C., Leung, K. K., Alfred, L., Tsang, R. C., Tsui, W. B., Fung, J. C., Ng, E. K., Cheung, S., Tang, A. W., and
660 Ning, Z.: Effects of synoptic patterns on the vertical structure of ozone in Hong Kong using lidar measurement,
661 *Atmos. Environ.*, 257, 118490, <https://doi.org/10.1016/j.atmosenv.2021.118490>, 2021.
- 662 Liu, F., Zhang, Q., van der A, R. J., Zheng, B., Tong, D., Yan, L., Zheng, Y., and He, K.: Recent reduction in NO_x
663 emissions over China: synthesis of satellite observations and emission inventories, *Environ. Res. Lett.*, 11, 114002,
664 <https://doi.org/10.1088/1748-9326/11/11/114002>, 2016.
- 665 Liu, H., Jacob, D. J., Chan, L. Y., Oltmans, S. J., Bey, I., Yantosca, R. M., Harris, J. M., Duncan, B. N., and
666 Martin, R. V.: Sources of tropospheric ozone along the Asian Pacific Rim: An analysis of ozonesonde
667 observations, *J. Geophys. Res.*, 107, ACH 3-1-ACH 3-19, <https://doi.org/10.1029/2001JD002005>, 2002.
- 668 Ma, Z., Xu, J., Quan, W., Zhang, Z., Lin, W., and Xu, X.: Significant increase of surface ozone at a rural site,
669 north of eastern China, *Atmos. Chem. Phys.*, 16, 3969-3977, <https://doi.org/10.5194/acp-16-3969-2016>, 2016.
- 670 Manney, G. L., and Hegglin, M. I.: Seasonal and regional variations of long-term changes in upper-tropospheric
671 jets from reanalyses, *J. Climate.*, 31, 423-448, <https://doi.org/10.1175/JCLI-D-17-0303.1>, 2018.
- 672 Meul, S., Langematz, U., Kröger, P., Oberländer-Hayn, S., and Jöckel, P.: Future changes in the stratosphere-to-
673 troposphere ozone mass flux and the contribution from climate change and ozone recovery, *Atmos. Chem. Phys.*,
674 18, 7721-7738, <https://doi.org/10.5194/acp-18-7721-2018>, 2018.
- 675 Miyazaki, K., Eskes, H., Sudo, K., Boersma, K. F., Bowman, K., and Kanaya, Y.: Decadal changes in global
676 surface NO_x emissions from multi-constituent satellite data assimilation, *Atmos. Chem. Phys.*, 17, 807-837,
677 <https://doi.org/10.5194/acp-17-807-2017>, 2017.
- 678 Morgenstern, O., Hegglin, M. I., Rozanov, E., O'Connor, F. M., Abraham, N. L., Akiyoshi, H., Archibald, A. T.,
679 Bekki, S., Butchart, N., Chipperfield, M. P., Deushi, M., Dhomse, S. S., Garcia, R. R., Hardiman, S. C., Horowitz,

680 L. W., Jöckel, P., Josse, B., Kinnison, D., Lin, M., Mancini, E., Manyin, M. E., Marchand, M., Marécal, V.,
681 Michou, M., Oman, L. D., Pitari, G., Plummer, D. A., Revell, L. E., Saint-Martin, D., Schofield, R., Stenke, A.,
682 Stone, K., Sudo, K., Tanaka, T. Y., Tilmes, S., Yamashita, Y., Yoshida, K., and Zeng, G.: Review of the global
683 models used within phase 1 of the Chemistry–Climate Model Initiative (CCMI), *Geosci. Model Dev.*, 10, 639–
684 671, <https://doi.org/10.5194/gmd-10-639-2017>, 2017.

685 Morris, G. A., Labow, G., Akimoto, H., Takigawa, M., Fujiwara, M., Hasebe, F., Hirokawa, J., and Koide, T.: On
686 the use of the correction factor with Japanese ozonesonde data, *Atmos. Chem. Phys.*, 13, 1243–1260,
687 <https://doi.org/10.5194/acp-13-1243-2013>, 2013.

688 Neu, J. L., Flury, T., Manney, G. L., Santee, M. L., Livesey, N. J., and Worden, J.: Tropospheric ozone variations
689 governed by changes in stratospheric circulation, *Nat. Geosci.*, 7, 340–344, <https://doi.org/10.1038/ngeo2138>,
690 2014.

691 Oltmans, S. J., Johnson, B. J., Harris, J. M., and Thompson, A. M.: Tropospheric ozone over the North Pacific
692 from ozonesonde observations, *J. Geophys. Res.*, <https://doi.org/10.1029/2003JD003466>, 2004.

693 Ploeger, F., and Birner, T.: Seasonal and inter-annual variability of lower stratospheric age of air spectra, *Atmos.*
694 *Chem. Phys.*, 16, 10195–10213, <https://doi.org/10.5194/acp-16-10195-2016>, 2016.

695 Plumb, R. A.: Stratospheric Transport, *J. Meteorol. Soc. Jpn.*, 80, 793–809, <https://doi.org/10.2151/jmsj.80.793>,
696 2002.

697 Ray, E. A., Moore, F. L., Elkins, J. W., Dutton, G. S., Fahey, D. W., Vömel, H., Oltmans, S. J., and Rosenlof, K.
698 H.: Transport into the northern hemisphere lowermost stratosphere revealed by in situ tracer measurements, *J.*
699 *Geophys. Res. Atmos.*, 104, 26565–26580, <https://doi.org/10.1029/1999JD900323>, 1999.

700 Revell, L. E., Stenke, A., Tummon, F., Feinberg, A., Rozanov, E., Peter, T., Abraham, N. L., Akiyoshi, H.,
701 Archibald, A. T., Butchart, N., Deushi, M., Jöckel, P., Kinnison, D., Michou, M., Morgenstern, O., O'Connor, F.
702 M., Oman, L. D., Pitari, G., Plummer, D. A., Schofield, R.,

703 Stone, K., Tilmes, S., Visioni, D., Yamashita, Y., and Zeng, G.: Tropospheric ozone in CCMI models and Gaussian
704 process emulation to understand biases in the SOCOLv3 chemistry–climate model, *Atmos. Chem. Phys.*, 18,
705 16155–16172, <https://doi.org/10.5194/acp-18-16155-2018>, 2018.

706 Roelofs, G.-J., and Lelieveld, J.: Model study of the influence of cross-tropopause O₃ transports on tropospheric
707 O₃ levels, *Tellus. B.*, 49, 38–55, <https://doi.org/10.3402/tellusb.v49i1.15949>, 1997.

708 Sander, R., Baumgaertner, A., Gromov, S., Harder, H., Jöckel, P., Kerkweg, A., Kubistin, D., Regelin, E., Riede,
709 H., Sandu, A., Taraborrelli, D., Tost, H., and Xie, Z. Q.: The atmospheric chemistry box model CAABA/MECCA-
710 3.0, *Geosci. Model Dev.*, 4, 373–380, <https://doi.org/10.5194/gmd-4-373-2011>, 2011.

711 Sander, R., Jöckel, P., Kirner, O., Kunert, A. T., Landgraf, J., and Pozzer, A.: The photolysis module JVAL-14,
712 compatible with the MESSy standard, and the JVal PreProcessor (JVPP), *Geosci. Model Dev.*, 7, 2653–2662,
713 <https://doi.org/10.5194/gmd-7-2653-2014>, 2014.

714 Shepherd, T. G., and McLandress, C.: A Robust Mechanism for Strengthening of the Brewer–Dobson Circulation
715 in Response to Climate Change: Critical-Layer Control of Subtropical Wave Breaking, *J. Atmos. Sci.*, 68, 784–
716 797, <https://doi.org/10.1175/2010JAS3608.1>, 2011.

717 Škerlak, B., Sprenger, M., Pfahl, S., Tyrlis, E., and Wernli, H.: Tropopause folds in ERA-Interim: Global
718 climatology and relation to extreme weather events, *J. Geophys. Res.*, 120, 4860–4877,
719 <https://doi.org/10.1002/2014JD022787>, 2015.

720 SPARC CCMVal: SPARC Report on the Evaluation of Chemistry Climate Models, edited by: Eyring, V.,
721 Shepherd, T. G., and Waugh, D. W., SPARC Report No. 5, WCRP-132, WMO/TD-No. 1526, [http://www.sparc-](http://www.sparc-climate.org/publications/sparc-reports/)
722 [climate.org/publications/sparc-reports/](http://www.sparc-climate.org/publications/sparc-reports/), 2010

723 Sprenger, M., Maspoli, M. C., and Wernli, H.: Tropopause folds and cross-tropopause exchange. A global
724 investigation based upon ECMWF analyses for the time period March 2000 to February 2001, *J. Geophys. Res.*,
725 108, <https://doi.org/10.1029/2002JD002587>, 2003.

726 Stohl, A., P. Bonasoni, P. Cristofanelli, W. Collins, J. Feichter, A. Frank, C. Forster, E. Gerasopoulos, H.
727 Gäggeler, P. James, T. Kentarchos, H. Kromp-Kolb, B. Krüger, C. Land, J. Meloan, A. Papayannis, A. Priller, P.
728 Seibert, M. Sprenger, G. J. Roelofs, H. E. Scheel, C. Schnabel, P. Siegmund, L. Tobler, T. Trickl, H. Wernli, V.
729 Wirth, P. Zanis, and Zerefos, C.: Stratosphere-troposphere exchange: A review, and what we have learned from
730 STACCATO, *J. Geophys. Res.*, <https://doi.org/10.1029/2002JD002490>, 2003.

731 Su, T., Li, J., Li, C., Xiang, P., Lau, A. K.-H., Guo, J., Yang, D., and Miao, Y.: An intercomparison of long-term
732 planetary boundary layer heights retrieved from CALIPSO, ground-based lidar, and radiosonde measurements
733 over Hong Kong, *J. Geophys. Res.*, 122, 3929–3943, <https://doi.org/10.1002/2016JD025937>, 2017.

734 Sudo, K., Takahashi, M., and Akimoto, H.: Future changes in stratosphere-troposphere exchange and their impacts
735 on future tropospheric ozone simulations, *Geophys. Res. Lett.*, 30, 2256, <https://doi.org/10.1029/2003GL018526>,
736 2003.

737 Sun, L., Xue, L., Wang, T., Gao, J., Ding, A., Cooper, O. R., Lin, M., Xu, P., Wang, Z., Wang, X., Wen, L., Zhu,
738 Y., Chen, T., Yang, L., Wang, Y., Chen, J., and Wang, W.: Significant increase of summertime ozone at Mount
739 Tai in Central Eastern China, *Atmos. Chem. Phys.*, 16, 10637-10650, <https://doi.org/10.5194/acp-16-10637-2016>,
740 2016.

741 Tost, H., Jöckel, P., Kerkweg, A., Sander, R., and Lelieveld, J.: Technical note: A new comprehensive
742 SCAVenging submodel for global atmospheric chemistry modelling, *Atmos. Chem. Phys.*, 6, 565-574,
743 <https://doi.org/10.5194/acp-6-565-2006>, 2006.

744 Tost, H., Jöckel, P., and Lelieveld, J.: Lightning and convection parameterisations – uncertainties in global
745 modelling, *Atmos. Chem. Phys.*, 7, 4553-4568, <https://doi.org/10.5194/acp-7-4553-2007>, 2007.

746 Trickl, T., Bärtsch-Ritter, N., Eisele, H., Furger, M., Mücke, R., Sprenger, M., and Stohl, A.: High-ozone layers
747 in the middle and upper troposphere above Central Europe: potential import from the stratosphere along the
748 subtropical jet stream, *Atmos. Chem. Phys.*, 11, 9343-9366, <https://doi.org/10.5194/acp-11-9343-2011>, 2011.

749 van der A, R. J., Mijling, B., Ding, J., Koukouli, M. E., Liu, F., Li, Q., Mao, H., and Theys, N.: Cleaning up the
750 air: effectiveness of air quality policy for SO₂ and NO_x emissions in China, *Atmos. Chem. Phys.*, 17, 1775-1789,
751 <https://doi.org/10.5194/acp-17-1775-2017>, 2017.

752 Verstraeten, W. W., Neu, J. L., Williams, J. E., Bowman, K. W., Worden, J. R., and Boersma, K. F.: Rapid
753 increases in tropospheric ozone production and export from China, *Nat. Geosci.*, 8, 690-695,
754 <https://doi.org/10.1038/NGEO2493>, 2015.

755 Wang, T., Xue, L., Brimblecombe, P., Lam, Y. F., Li, L., and Zhang, L.: Ozone pollution in China: A review of
756 concentrations, meteorological influences, chemical precursors, and effects, *Sci. Total Environ.*, 575, 1582-1596,
757 <https://doi.org/10.1016/j.scitotenv.2016.10.081>, 2017.

758 Williams, R. S., Hegglin, M. I., Kerridge, B. J., Jöckel, P., Latter, B. G., and Plummer, D. A.: Characterising the
759 seasonal and geographical variability in tropospheric ozone, stratospheric influence and recent changes, *Atmos.*
760 *Chem. Phys.*, 19, 3589-3620, <https://doi.org/10.5194/acp-19-3589-2019>, 2019.

761 Witte, J. C., Thompson, A. M., Smit, H. G. J., Vömel, H., Posny, F., and Stübi, R.: First Reprocessing of Southern
762 Hemisphere Additional OZonesondes Profile Records: 3. Uncertainty in Ozone Profile and Total Column, *J.*
763 *Geophys. Res.*, 123, 3243-3268, <https://doi.org/10.1002/2017JD027791>, 2018.

764 World Meteorological Organization: *Meteorology: A three dimensional science*, 6, 134–138, 1957.

765 Xu, W., Lin, W., Xu, X., Tang, J., Huang, J., Wu, H., and Zhang, X.: Long-term trends of surface ozone and its
766 influencing factors at the Mt Waliguan GAW station, China – Part 1: Overall trends and characteristics, *Atmos.*
767 *Chem. Phys.*, 16, 6191-6205, <https://doi.org/10.5194/acp-16-6191-2016>, 2016.

768 Young, P. J., Naik, V., Fiore, A. M., Gaudel, A., Guo, J., Lin, M. Y., Neu, J. L., Parrish, D. D., Rieder, H. E.,
769 Schnell, J. L., Tilmes, S., Wild, O., Zhang, L., Ziemke, J., Brandt, J., Delcloo, A., Doherty, R. M., Geels, C.,
770 Hegglin, M. I., Hu, L., Im, U., Kumar, R., Luhar, A., Murray, L., Plummer, D., Rodriguez, J., Saiz-Lopez, A.,
771 Schultz, M. G., Woodhouse, M. T., and Zeng, G.: Tropospheric Ozone Assessment Report: Assessment of global-
772 scale model performance for global and regional ozone distributions, variability, and trends, *Elem. Sci. Anth.*, 6,
773 <https://doi.org/10.1525/elementa.265>, 2018.

774 Zeng, G., and Pyle, J. A.: Influence of El Niño Southern Oscillation on stratosphere/troposphere exchange and the
775 global tropospheric ozone budget, *Geophys. Res. Lett.*, 32, <https://doi.org/10.1029/2004GL021353>, 2005.

776 Zhang, Y., Liu, H., Crawford, J. H., Considine, D. B., Chan, C., Oltmans, S. J., and Thouret, V.: Distribution,
777 variability and sources of tropospheric ozone over south China in spring: Intensive ozonesonde measurements at
778 five locations and modeling analysis, *J. Geophys. Res.*, 117, <https://doi.org/10.1029/2012JD017498>, 2012.

779 Zhang, Y., Cooper, O. R., Gaudel, A., Thompson, A. M., Nédélec, P., Ogino, S.-Y., and West, J. J.: Tropospheric
780 ozone change from 1980 to 2010 dominated by equatorward redistribution of emissions, *Nat. Geosci.*, 9, 875-879,
781 <https://doi.org/10.1038/ngeo2827>, 2016.

782 Zhao, K., Huang, J., Wu, Y., Yuan, Z., Wang, Y., Li, Y., Ma, X., Liu, X., Ma, W., Wang, Y., and Zhang, X.:
783 Impact of stratospheric intrusions on ozone enhancement in the lower troposphere and implication to air quality
784 in Hong Kong and other South China regions, *J. Geophys. Res.*, 126, e2020JD033955,
785 <https://doi.org/10.1029/2020JD033955>, 2021.

786 Zhou, D., Ding, A., Mao, H., Fu, C., Wang, T., Chan, L. Y., Ding, K., Zhang, Y., Liu, J., Lu, A., and Hao, N.:
787 Impacts of the East Asian monsoon on lower tropospheric ozone over coastal South China, *Environ. Res. Lett.*, 8,
788 044011, <https://doi.org/10.1088/1748-9326/8/4/044011>, 2013.

789